Warburg-like effect is a hallmark of complex I assembly defects

Valerie Desquiret-Dumas, Geraldine Leman, Celine Wetterwald, Stephanie Chupin, Anaïs Lebert, Salim Khiati, Morgane Le Mao, Guillaume Geffroy, Mariame Selma Kane, Arnaud Chevrollier, et al.

Warburg-like effect is a hallmark of complex I assembly defects

Running title: **Mitochondrial Complex I assembly drives cell metabolic fate**

Valerie Desquiret-Dumas[1,2], Geraldine Leman[1], Celine Wetterwald[2], Stephanie Chupin[2], Anaïs Lebert[1], Salim Khiati[1], Morgane Le Mao[1], Guillaume Geffroy[1], Mariame Selma Kane[1], Arnaud Chevrollier[1], David Goudenege[1], Cedric Gadras[2], Lydie Tessier[2], Magalie Barth[1,2], Stephanie Leruez[2], Patrizia Amati-Bonneau[1,2], Daniel Henrion[1], Dominique Bonneau[1,2], Vincent Procaccio[1,2], Pascal Reynier[1,2], Guy Lenaers[1], Naig Gueguen[1,2]

[1] UMR CNRS 6015-INSERM U1083, MitoVasc Institute, University of Angers, Angers, France

[2] Department of Biochemistry and Genetics, University Hospital of Angers, F-49000, France

Corresponding author: NaGueguen@chu-angers.fr

SUMMARY

Due to its pivotal role in NADH oxidation and ATP synthesis, mitochondrial complex I (CI) emerged as a crucial regulator of cellular metabolism. A functional CI relies on the sequential assembly of nuclear- and mtDNA-encoded subunits; however, whether CI assembly status is involved in the metabolic adaptations in CI deficiency still remains largely unknown. Here, we investigated the relationship between CI functions, its structure and the cellular metabolism in 29 patient fibroblasts representative of most CI mitochondrial diseases. Our results show that, contrary to the generally accepted view, a complex I deficiency does not necessarily lead to a glycolytic switch, i.e. the so-called Warburg effect, but that this particular metabolic adaptation is a feature of CI assembly defect. By contrast, a CI functional defect without disassembly induces a higher catabolism to sustain the oxidative metabolism. Mechanistically, we demonstrate that reactive oxygen species overproduction by CI assembly intermediates and subsequent AMPK-dependent Pyruvate Dehydrogenase inactivation are key players of this metabolic reprogramming. Thus, this study provides a two-way-model of metabolic responses to CI deficiencies that are central not only in defining therapeutic strategies for mitochondrial diseases, but also in all pathophysiological conditions involving a CI deficiency.

KEYWORDS

complex I deficiency; complex I assembly; mitochondrial metabolism; metabolic reprogramming; ROS production.

INTRODUCTION

A metabolic transition towards glycolysis in aerobic conditions, the so-called Warburg effect, is a hallmark of many pathological conditions not only in cancer cells but also in systemic diseases or in metabolic disorders. However, to date it remains unclear how cells engage the aerobic glycolysis at the expense of oxidative phosphorylation. In cancer cells, recent data converge to the concept that mitochondrial complex I (CI) is a crucial regulator of cellular metabolic fate [1-5]. Indeed, through its activity, consisting in NADH oxidation coupled to quinone reduction and protons pumping, CI contributes to the NAD+/NADH equilibrium, the ADP/ATP ratio and ROS production [6, 7], all key modulators of the cellular metabolic orientation [8-12].

CI deficiency is the most frequent defect encountered in mitochondrial disorders [13]. Its clinical presentations (OMIM #252010) are highly variable among patients ranging from isolated organ failures, as the Leber Hereditary Optic Neuropathy (LHON OMIM #535000) affecting the optic nerve, to multivisceral failure as the Leigh syndrome (OMIM #256000). CI deficiency is also the pre-eminent feature of the MELAS syndrome (Myopathy, Encephalopathy, Lactic Acidosis and Strokes, OMIM #540000), mainly due to the m.3243A>G pathogenic variant in the mitochondrial tRNA (MT-TRNA) Leucine 1 (*MT-TL1*) [14]. Although it is commonly assumed that CI deficiencies are associated with an upregulation of aerobic glycolysis, this clinical heterogeneity increasingly challenges this assumption and questions whether the metabolic transition is really engaged proportionally to the degree of CI enzymatic defect. CI diseases are indeed commonly considered as a defect in CI activity. However, beyond these functional defects, increasing literature reports novel CI pathogenic variants compromising CI assembly [15, 16], a parameter yet underestimated in the pathophysiology of CI deficiency.

The structure of this large L-shaped complex of 44 subunits combines a matrix arm composed of two functional domains, the N (NADH binding) and Q (Quinone binding) modules and a membrane arm corresponding to the P (Proton pumping) module. The catalytic core subunits of the P-module are encoded by the mitochondrial DNA (MT-DNA), while the N and Q modules are exclusively encoded by the nuclear DNA (nDNA). Recent findings led to a consensus modular assembly model that involves the independent building of submodules, and their step-by-step association (Supplementary Figure 1A). This process is assisted by at least 13 assembly factors specific of each module [17, 18] that dissociate from the complex once finally assembled. Defects in this intricate assembly process would lead to the accumulation of CI assembly subcomplexes unconnected from each other's, which could be deleterious for the cell [19], therefore questioning the involvement of such a defect in metabolic rewiring.

Thus, a comprehensive analysis of the pathophysiological consequences of CI deficiencies is required for a better understanding of the mechanisms linking CI function, assembly and metabolic adaptations and is a pre-requisite for the development of therapeutic strategies. To address this question, we took advantage of a large skin fibroblast collection obtained from patients presenting CI deficiency, with impairment in CI functionality and/or assembly. Our results shed light on the CI assembly status as a highly discriminative parameter in the metabolic adaptation to CI deficiencies and position ROS and PDH phosphorylation as key mediators of the glycolytic switch related to CI assembly defects.

MATERIAL AND METHODS

EXPERIMENTAL MODELS

Study approval

This work was approved by the Ethics Committee of the Angers University Hospital (CPP Ouest II – Angers, France; Identification number: CPP CB 2014/02; Declaration number: DC-2011-1467 and Authorization number: AC-2012-1507). Written informed consent was obtained from all participants. The description of the mutations from each patient and their phenotype are detailed in Supplementary Figure 2.

Cell lines and cell culture

Fibroblasts obtained from skin biopsy from 40 individuals, 29 patients with CI deficiency and 11 healthy controls (Supplementary Figure 2) were cultured in 2/3 Dulbecco's modified Eagle medium (DMEM-F12, PAN Biotech, Wimborne, UK), 1/3 Amniomax (Gibco, Invitrogen, Paisley, UK) supplemented with 10% fetal bovine serum (PAN Biotech, Wimborne, UK), 1 mM sodium pyruvate, and 50 µg/ml uridine (Sigma Aldrich, Lyon, France) at 37◦C, 5% CO_2. One week before analyses, uridine and pyruvate supplementations were stopped to avoid any influence of high pyruvate concentration on the cellular metabolism. All experiments were conducted on fibroblast cultures between passages 6 and 25 to avoid artefacts due to senescence [20]. All fibroblast cell lines were routinely tested for the absence of mycoplasma contamination. For experiments, cells were washed with PBS, trypsinized, centrifugated (800 rpm, 5 min), washed in PBS buffer and the cell pellets were either immediately used

(oxygraphic analysis, NAD+/NADH measurement) or immediately frozen in liquid nitrogen and stored at -80°C until use.

METHODS

Cell treatments and Small Interference RNA

To induce CI assembly defect, fibroblasts from healthy controls were treated during 48h with 1µM sodium Pyrithione (2-Mercaptopyridine-*N*-oxide sodium, NaPyr, Sigma Aldrich, Saint-Quentin Fallavier, France). NaPyr solutions in DMSO were diluted 1:5,000 in the cell culture medium (without uridine or pyruvate supplementation). Control cells were treated in parallel with DMSO 1:5,000 ("vehicle" condition).

To inhibit CI activity, cells were treated during 48h with Piericidin A, 5 nM (Sigma Aldrich, Saint-Quentin Fallavier, France). Piericidin A stock solutions in DMSO were diluted 1:5,000 in the medium. Control cells were treated in parallel with DMSO diluted 1:5,000 in the medium ("vehicle" condition). Importantly, Piericidin A was chosen instead of the classical CI inhibitor, rotenone, due to the higher dynamic range between CI inhibition and induction of reactive oxygen species (ROS) production of piericidin A [21]. Dose-response titrations (2.5 nM up to 50 nM) with both rotenone and piericidin A were performed on control fibroblasts before cell treatment and CI-inhibition and CI-linked ROS production were analyzed simultaneously using O2K-fluorometry by measuring both the CI-linked maximal respiration and CI-linked Amplex red oxidation on the same sample (see below: Mitochondrial ROS production section). The dose of Piericidin A was chosen as the one that induced the closest inhibition of CI-linked respiration than the one observed on CI patient cells (i.e. -59.8 ± 2.2%) without inducing a ROS production. At the chosen dose (5 nM), piericidin A inhibited both CI-linked respiration (-65%) and ROS production (-29%) while 5

nM of rotenone only inhibited CI-linked maximal respiration by -24% without inducing ROS production. At 50 nM, both inhibitors fully inhibited CI-linked respiration (-99 and -88% for piericidin A and rotenone, respectively) but strongly stimulated ROS production (+75 and +344% for piericidin A and rotenone, respectively).

Silencing of NDUFAF1 was performed on control fibroblasts by using a pool of three specific siRNA duplexes (Thermofisher, Waltham, USA). Control fibroblasts were reverse transfected using the Mission siRNA reagent (Sigma Aldrich, Saint Quentin Fallavier, France) and 40pmol of NDUFAF1 or control siRNA (scramble). After 48 hours, cells were harvested and oxygraphic analysis was performed. A frozen pellet was kept at -80°C for Western blot and BN PAGE and an aliquot of cell culture medium was frozen for metabolite measurements (see below).

To induce ROS production by CI, control cells were treated during 48h with 5 µM mitochondria-targeted redox cycler, MitoParaquat (mt-PQ, Abcam, Cambridge, UK). Within the matrix, MitoPQ produces superoxide by redox cycling at the flavin site of complex I, selectively increasing superoxide production within mitochondria [22]. A 25 mM mt-PQ stock solution in DMSO was diluted 1:5,000 in the medium. Control cells were treated in parallel with DMSO diluted 1:5,000 in the medium ("vehicle" condition).

Cellular antioxidant treatments were conducted using N-Acetyl cysteine (NAC, 48H, 1mM, Sigma Aldrich, Saint Quentin Fallavier, France). A fresh 100 mM NAC solution was realized in DMEM-F12 medium for each experiment and diluted at 1:100 in the final cell culture medium. Control cells were treated in parallel with DMEM-F12 diluted 1:100 in the cell culture medium ("vehicle" condition).

AMPK inhibition in patient and control cells was performed using Compound C (Abcam, Cambridge, UK) (48H, 10 µM). A 10 mM stock solution in DMSO was diluted 1:1,000 in the medium. Cells were treated in parallel with DMSO diluted 1:1,000 in the medium ("vehicle" condition).

Mitochondrial enzymatic activities

The activities of Complex I (NADH ubiquinone reductase, NUR, EC 1.6.5.3) and citrate synthase (CS, EC 2.3.3.1) were measured at 37°C with a UV*mc*^{2} spectrophotometer (SAFAS, Monaco) on mitochondrial enriched fraction. Cells were re-suspended in cell buffer (250 mM saccharose, 20 mM tris[hydroxymethyl]aminomethane, 2 mM EGTA, 1 mg/mL bovine serum albumin, pH 7.2; 50 µl/10^6 cells), disrupted by two freezing-thawing cycles, washed, centrifuged for one minute at 16 000 g to eliminate the cytosolic fraction, re-suspended in the cell buffer (250 µl/10^6 cells) and sonicated (6×5 s) on ice. Complex I activity was immediately assayed according to [23, 24] in KH_2PO_4 buffer (80 mM, pH 7.4) supplemented with 1mg/ml fatty acid free bovine serum albumin, 1 mM potassium cyanide (KCN), 2 mM sodium azide (NaN3) and 100 µM DCPIP added to maintain the quinone acceptor in fully oxidized state, thus avoiding NUR reaction inhibition by reduced $CoQH_2$ accumulation [25]. 100 µM Coenzyme Q1 (Sigma Aldrich, Saint Quentin Fallavier, France) were used as acceptor and 150 µM NADH as substrate to initiate the reaction. The specificity of the NUR reaction was controlled on the same sample in the presence of its specific inhibitor, rotenone (5 µM). Citrate synthase activity was assayed by a standard procedure [23, 24]. The protein content was determined with the bicinchoninic assay kit (Uptima, Interchim, Montluçon, France) using bovine serum albumin as standard. CI activity was normalized to CS as a mitochondrial content marker, after checking for the absence of difference in the

mitochondrial CS activity between groups. Enzymatic measurements were performed at least twice in duplicate, on two different cell pellets from different passages.

Mitochondrial respiration rates

Mitochondrial oxygen consumption measurements were performed at 37◦C and atmospheric pressure using a high-resolution oxygraph (O2K, Oroboros Instrument, Innsbruck, Austria). Respiration rates on permeabilized cells were measured in respiratory buffer RB (10mM KH_2PO_4, 300mM mannitol, 10mM KCl, 5mM $MgCl_2$, 0.5mM EGTA and 1 mg/ml serum albumin bovine, pH7.2) using substrates of CI, CI+CII and CII as followed: first, state 2 (non-phosphorylating) respiration was measured after adding 2.5mM pyruvate and 5mM malate. Then, the CI-linked maximal phosphorylating respiration was stimulated by saturating ADP concentration (1.5mM) and 3mM NAD+, added to avoid TCA limitation by NAD+ availability. Succinate (10mM) was then added to measure the combined CI and CII-linked respiration with convergent CI+II electron flow into the Q-junction corresponding to the maximal stimulated phosphorylating respiration (OXPHOS capacity). Rotenone (5µM) was used to inhibit CI activity and thus to obtain the maximal CII-linked respiration. Thirdly, oligomycin (F0F1-ATP synthase inhibitor, 4µg/ml) and FCCP (carbonyl cyanide p-trifluoromethoxyphenylhydrazone, a mitochondrial uncoupler, 1µM) were sequentially added to ensure that the cells were fully permeabilized. Finally, antimycin A addition (2µg/ml) was used to check for the non-mitochondrial oxidation.

Respiration rates on intact cells were measured in DMEM-F12 medium (3g/l glucose, 1mM glutamine, 0.3mM pyruvate). 4-5.10^6 cells were added in the oxygraphic chamber and the analysis started with routine respiration (R) measurement, which is defined as respiration in DMEM-F12 medium without additional substrates or effectors (cell endogenous respiration, corresponding to the cellular oxidative metabolism). Then, F0F1-ATP synthase was inhibited

with oligomycin (4 µg/ml), allowing the measurement of non-phosphorylating respiration (Leak respiration). This non-phosphorylating respiration (O) was subtracted from Routine (R) one to calculate the cellular phosphorylating respiration (R-O). This was followed by uncoupling of oxidative phosphorylation by stepwise titration of FCCP (carbonyl cyanide p-trifluoromethoxyphenylhydrazone) up to optimum concentrations (0.6 – 1.2 µM) allowing the measurement of the maximal endogenous respiration (cellular oxidative capacity). The part of the maximal capacity use for oxidative metabolism was calculated as R/F and the part of the maximal capacity use for oxidative ATP synthesis was calculated as (R-O)/F. Finally, respiration was inhibited by rotenone and antimycin A (2.5µM and 2 µg/ml, respectively) to check for non-mitochondrial oxidation. All experiments were performed at least twice in duplicate on independent cell cultures.

Mitochondrial ROS production

ROS production was measured simultaneously to oxygen consumption at 37◦C and atmospheric pressure in respiratory buffer RB using the O2k-Fluorometer (Oroboros Instrument, Innsbruck, Austria) equipped with two-channel fluorescence optical setup to monitor oxygen level and fluorescence. H_2O_2 production was monitored according to [26] using the H_2O_2-sensitive probe Amplex® Red (Molecular Probes, Eugene, Oregon, USA), 10µM (Excitation 525nm / Emission filter 580nm). 1U/mL horse radish peroxidase (HRP) and 5U/mL superoxide dismutase (SOD) were added to the chamber to convert superoxide into H_2O_2. Calibrations were carefully performed before, during and at the end of each experiment with stepwise additions of 0.1µM H_2O_2. Dedicated CI and CI+CII-linked ROS production was sequentially analysed on the same sample using substrates of CI, CI+CII and CII as followed: first, NADH supply to CI was induced by adding 2.5mM pyruvate and 5mM malate (+ADP, 1.5mM). Then, NADH supply was further increased by addition of 5mM

glutamate. Finally, Succinate (10mM) was added to measure the ROS production with convergent CI+II electron flow into the Q-junction, corresponding to the maximal stimulated phosphorylating respiration. Specific H_2O_2 fluxes were calculated in real-time using the DatLab software (OROBOROS Instruments, Innsbruck, Austria) from the positive time derivative of the resorufin signal over time.

TCA cycle analysis

Oxidation of CI substrates was followed on 6-7.10^6 permeabilized fibroblasts. 2.5mM pyruvate and 5mM malate were added and a 1ml aliquot was immediately removed for acid organic analysis. Five minutes after substrate addition, sub-saturating ADP concentration (0.5mM) was added. Precisely 30 minutes later, a new 1ml aliquot was withdrawn. Oxygen consumption was controlled during all the experiment. Both aliquots were treated with 200µl of 7% perchloric acid then rapidly stirred, frozen in liquid nitrogen and thawed at 37°C, centrifuged 5 minutes at 20,000g, 4°C. Supernatants were extracted by ethyl acetate (1/7 v/v), evaporated, silylated (45 minutes, 80°C) and injected in a gas chromatography/mass spectrophotometer (GCMS-2010C, Shimadzu, Marne la Vallée, France). Peaks were identified and quantified by the GCMS solution software (Shimadzu, Marne La Vallée, France).

Western blotting and BN-PAGE analysis

Cellular proteins solubilized in a Laemmli buffer were resolved by SDS-PAGE as described [27].

For complex I and supercomplexes assembly analyses, mitochondria were enriched by using differential centrifugation, according to a slightly modified version of the method described by Bonnet et al (2008). Briefly, the cell pellets were incubated 10 min on ice with cold

digitonin (4mg/ml in PBS, v/v; 0.2% w/v) to dissolve cell membranes. Then, digitonin was diluted by addition of cold PBS (5 v/v). Cells were centrifugated for 10 min, at 10,000g and 4 °C to recover the mitochondria-enriched fraction. The pellet was washed once more in 1 ml cold PBS, centrifuged (10,000g, 4°C), resuspended at 10 mg/ml in AC/BT buffer (1.5 M aminocaproic acid and 75 mM Bis–Tris/HCl, pH 7.0, supplemented with Complete Mini Protease Inhibitor (Roche Diagnostics, Stockholm, Sweden)) and kept frozen at -80°C until analysis. For blue native (BN) PAGE analyses, 50 µg of the samples were diluted at 2 mg/ml in AC/BT buffer and mitochondrial membrane proteins were solubilized by incubation with the dedicated detergent for 10 minutes at 4°C. After centrifugation for 20 minutes, 20,000g at 4°C, the supernatant was collected, and 5% Serva Blue G dye (Biorad, Marnes-la-Coquette, France) in 1 M aminocaproic acid/50 mM Bis–Tris/HCl, pH 7 was added (1/20 v/v) prior to loading. The following detergents were used (a) 3g/g protein n-dodecyl β-d-maltoside for preparation of native respiratory chain complexes and (b) 6 g/g protein digitonin (1.2% w/v) to detect the supercomplexes. Respiratory chain complexes or supercomplexes were separated on Native PAGE Novex 3-12% Bis-Tris gels (Invitrogen) for approximatively 3 hours and transfered on PVDF membranes (GE Healthcare, Velizy-Villacoublay, France) in cold blotting buffer (25 mM Tris, 192 mM glycine, pH 8.3, 20% methanol). Membranes were hybridized using dedicated monoclonal antibodies (NDUFS2, NDUFB6, SDHA, III core2, COX5A, Abcam). Due to the reduced dynamic range of chemiluminescence, the high intensity of the CI holoenzyme band could blunt the CI intermediate detection. Thus, to avoid this limitation, we developed a new approach based on the detection of assembly factors that specifically bind to CI intermediates and are removed once the holoenzyme is fully assembled. Antibodies against assembly factors NDUFAF4 (Rabbit monoclonal antibody, Abcam) that specifically bind the Q and Q/Pp-a, NDUFAF1 (Rabbit monoclonal antibody, Abcam) which binds the membrane Pp-b and NDUFAF2 (Rabbit monoclonal antibody,

Abcam) which stacks the Q/P intermediates, were used after careful validation of the method (see Supplementary Figure 1). Acquisitions were performed using the Odyssey FC imaging system and analysed using Image Studio™ Lite (LI-COR Biosciences).

Metabolites measurements

Cellular glucose consumption and lactate production were determined on cell supernatant after 48 hours of cell culture on an Architect C16000 apparatus using the Glucose assay for Architect C™ system and the Lactate assay for Architect C™ system (Abbott, Ringis, France). Cellular NAD+/NADH ratio and ADP/ATP ratio were measured on cell lysates according to the manufacturer instructions (NAD/NADH assay kit and ADP/ATP ratio assay kit, Abcam, Cambridge, UK).

QUANTIFICATION AND STATISTICAL ANAYSIS

At least two biological replicates of each fibroblast cell line were analyzed in duplicate. All fibroblasts cell lines were systematically analyzed (Ctr, n=11; FA, n=19; AB, n=10), except when specified. Results are represented as mean ± *SEM*. The nonparametric Mann–Whitney test (*, $ symbols) or its version for paired data (Wilcoxon test, # symbols) were used for means comparison (Statview, SAS Institute Inc., Cary NC, USA). All data were considered statistically significant at $p<0.05$. For regression analyses, the best fitting model and the statistical significance were determined using SigmaPlot software (Systat Software, Inc., San Jose, USA) using *t* test and *F* test for the regression significance.

Principal component analysis (PCA) score plot was conducted to detect grouping of similar cell lines and outliers according to structural, biochemical and metabolic parameters (X matrix). An orthogonal partial least-squares discriminant analysis (OPLS-DA), a supervised pattern-recognition method, was further used to maximize the variation between groups and

determine the most significant variables contributing to this variation. The quality of models was validated by determining R^2 (goodness-of-fit) and Q^2 (goodness-of-prediction) values. In the model with the best predictive capabilities, the significant variables of orthogonal partial least-squares discriminant analysis models can be detected and selected by plotting VIP versus coefficient values ("volcano" plot). VIP values summarize the importance of each variable for the OPLS-DA model, while coefficient values summarize the relationship between the Y (groups) and X (matrix of measured parameters) variables. Variables with a VIP value ≥ 1 are considered important for group discrimination in predictive models. The multivariate data analysis was conducted using SIMCA-P software 13.0 (Umetrics, Umeå, Sweden).

RESULTS

Different metabolic rewirings are set to face CI deficiencies.

First, we checked the CI maximal activity (Supplementary information, Fig. S3A1) and maximal CI-linked respiration (St3 MP, Supplementary information, Fig. S3A2) of our cohort of 29 CI patient fibroblast cell lines and 11 controls (Supplementary information Fig. S2A). As expected, NADH Ubiquinone Reductase activity was decreased in all CI-mutated cell lines, except in the MT-ND4 and MT-TL cells with the Lowest heteroplasmy Levels (LL, i.e. MT-TL1.1 and MT-TL1.2, Supplemental information S2A Supplementary information, Fig. S3A1). By contrast, the maximal CI-linked respiration was reduced for all patient cell lines by at least 40% (Supplementary information Fig. S3A2), emphasizing a defect in CI function for all CI mutant cells. We then checked the maximal oxidative phosphorylation (OXPHOS) capacity by measuring the combined CI+CII phosphorylating respiration (St3 MPS, Supplementary information Fig. S3B). This parameter was not significantly reduced (-20 to -

30%), except for MT-TL and MT-TK cells (-60%). This latter particular feature of MT-TRNA mutated cells may be accounted for the additional decreased in both complexes IV and V activities (-60 and -70%, respectively, (data not shown), limiting the phosphorylating capacity. The relatively preserved maximal OXPHOS capacity witnessed that nearly all cells were able to compensate the CI deficiency by $FADH_2$ oxidation through CII, when its substrate is provided in excess.

Then, we characterized the balance between oxidative and glycolytic metabolism of the CI patient and control fibroblast cells (Fig. 1A, Supplementary information, Fig S3). Cellular oxidative metabolism was analysed by measuring on intact cells the routine (Routine, Supplementary information, Fig. S3C1) and the phosphorylating respirations (Routine - Oligomycin-insensitive respiration, R-O, Supplementary information, Fig. S3C2). Maximal respiratory chain capacity was measured after respiration uncoupling using FCCP (F, Supplementary information, Fig. S3D) and the relative use of the maximal capacity to sustain oxidative phosphorylation was calculated as the (R-O)/F ratio (Supplemental information, Fig. S3E). In parallel, we estimated the glycolytic metabolism by measuring the glucose conversion to lactate (L/G ratio, Supplementary information, Fig. S3F). Finally, these two parameters were represented on a same graph named metabolic orientation which represented one a same graph bar the use of glycolytic (L/G ratio) and oxidative ((R-O)/F) capacities in percent of control cells (Fig. 1A). Importantly, the metabolic balance was switched towards aerobic glycolysis only in a subset of mutated cells (Fig. 1A, Supplementary information Fig. S3E and S3F), suggesting different metabolic reprogramming among CI deficient cells.

To statistically process all the aforementioned data, we performed a non-supervised principal component analysis (PCA-X, Fig. 1B). The resulting model showed strong fitting (R^2X = 0.722) capabilities, distinguishing two groups among the CI-deficient cells which were

separated according to their metabolic orientation (x-axis: left side, L/G *vs* right side, R, R-O and R-O/F, Fig. 1B). The group A included all *MT-ND, MT-TL LL, MT-TP, NDUFV1.1, NDUFS4.1* and *NDUFA9* mutated cells while the group B encompassed all nDNA mutated cells, with the exception of *NDUFA9, NDUFV1.1* and *NDUFS4.1*, and the *MT-TK* and *MT-TL* with the Highest heteroplasmy Level (HL, MT-TL1.3 and MT-TL1.4, Supplementary information S2A) (hierarchical clustering, Supplementary information Fig. S3G). To gain insights in the discriminating parameters, we performed a supervised analysis (OLPS-DA, Fig. 1C1) based on these two groups defined by PCA. The Volcano plot (Fig. 1C2) confirmed that the most discriminative parameters between the two groups were the oxidative metabolism (R, R-O, R-O/F, VIP >1) *vs* the glycolytic metabolism (L/G)), while CI functionality (St3 MP and CI/CS) only accounted for a minor weight in the model (VIP <0.9). In the light of these analyses, we reconsidered our data according to the different groups defined by the PCA analysis.

In the group A, the oxidative metabolism (Routine and phosphorylating (R-O) respirations Fig. 1D1 and 1D2) was maintained thanks to the use of a higher part of the spare capacity ((R-O)/F, +30%, Fig. 1D3, Supplemental Figure 3H) and the glycolysis was barely increased (increase in glucose consumption and lactate production, Fig. 1E1 and increase in L/G: +27%, Fig. 1E2). By contrast, the oxidative metabolism was significantly decreased in the group B (Routine - 47% and phosphorylating respiration, R-O, - 60% compared to Ctr, Fig. 1D1 and 1D2, Supplemental Figure 3H). Surprisingly, these cells did not used and even reduced the use of their respiratory capacity to maintain oxidative phosphorylation, as illustrated by the decreased (R-O)/F ratio (-40%, Figure 1D3, Supplemental Figure 3H), substantiating a clear shutdown of the oxidative metabolism in the group B. Simultaneously, in these cells, glucose was almost exclusively converted to lactate (Fig. 1E1), as indicated by a L/G ratio close to 2

(+77%, Fig. 1E2, Supplemental Figure 3H). In addition, we found a low cellular ATP/ADP ratio (-55% compared to Ctr and group A, Fig. 1F) that was not modified by the inhibition of the phosphorylating respiration (+ Oligomycin), confirming that the ATP synthesis in the group B is mainly supported by the glycolytic metabolism. Altogether, these results revealed two different metabolic adaptations: in the group A, both the oxidative and glycolytic metabolisms are slightly stimulated, while the equilibrium between them is maintained (metabolic orientation, glycolytic *vs* oxidative metabolisms, i.e. L/G *vs* (R-O)/F, Fig. 1G), evidencing a hyper-catabolism. Conversely, in the group B, the metabolism is drastically switched toward aerobic glycolysis at the expense of the oxidative phosphorylation, namely the Warburg effect (Fig. 1G).

It is generally thought that the glycolytic switch is linked to the degree of CI deficiency. However, while CI activity was more decreased in B than in the A group, no difference in the degree of CI-linked respiration deficiency was observed between the two patient groups (Fig. 1H1 and 1H2). Moreover, neither the CI activity nor the CI supported maximal respiration rate correlated with the metabolic orientation, confirming that these parameters are not discriminant in the observed metabolic adaptations (Fig. 1I1 and 1I2). CI activity is also a crucial regulator of NAD^+/NADH ratio [23]. This ratio was decreased in both groups, compared to Ctr (Fig. 1J) but was neither different between the two groups nor correlated to the CI holoenzyme quantity (Fig. 1K), excluding a regulation of metabolic rewiring by NAD+/NADH ratio.

CI assembly is a key determinant of metabolic rewiring in CI deficient cells.

The location of the mutated subunits within CI could not only affect its activities (NADH oxidation, proton pumping) but also its structure. Thus, we evaluated by Blue Native PAGE the impact of the different mutations on CI assembly (Fig. 2A and Supplementary

information, Fig. 4A, B). CI holoenzyme was detected by using antibodies targeting structural CI subunits (NDUFS2 and NDUFB6). CI intermediates were revealed with chaperon targeted antibodies (NDUFAF4, NDUFAF1 and NDUFAF2) that bind the matrix arms (Q and Q/Pp-a), the membrane arm (Pp-b) and the 830kDa intermediates, respectively (Supplementary information, Fig. 1B). The analysis revealed two CI assembly profiles (Figure 2A, 2B and Supplementary information, Fig. S4A). Firstly, in group A, CI holoenzyme quantity was not decreased by more than thirty percent (Fig. 2A, 2B1 and Supplementary information, Fig. S4A1) while no significant accumulation of CI intermediates was evidenced (Fig. 2A, 2B1 and Supplementary information, Fig. S4A2) and the equilibrium between CI holoenzyme and assembly intermediates was maintained (Fig. 2B2). This group was thus renamed FA for Fully Assembled. Secondly, in group B, CI holoenzyme quantity was markedly reduced (Fig. 2A, 2B1 and Supplemental information, Fig. S4A) and either matrix (Q/Pp-a, MT-TRNA cells), membrane (Pp-b, nDNA) or membrane and late-stage (Q/P, N-module mutated cells) intermediates accumulated (Supplemental information, Fig. 4B). Whatever the blocking step involved, these data emphasized a strong CI assembly defect in B group (Fig. 2B2). This group was renamed AB for Assembly Blockage. Importantly, the level of assembly defects strongly correlated with the metabolic rewiring (Fig. 2C, R^2=0.83), meaning that when the quantity of the CI holoenzyme is reduced, the metabolic orientation is proportionally switched towards glycolysis. Moreover, the supervised analysis according to the defined groups and the corresponding Volcano plot (Supplemental information, Fig. 4C) confirmed that the most discriminative parameters between the two groups are the CI assembly status (CI holoenzyme quantity (CI) *vs* the accumulation of assembly intermediates (A.I.)).

As our results question the common idea that the CI functions dictate the metabolic adaptations, we strengthened our analysis by selecting all the cell lines that displayed strictly

the same CI functionality (CI maximal activity and CI-linked maximal respiration) and comparable maximal phosphorylating capacity, thus differing only by their CI assembly level (Fig. 2D). Among them, only the ones with a CI assembly blockage showed a decreased use of respiratory spare capacity ((R-O)/F, -50%) and an increased use of glycolytic metabolism (L/G +50%, Supplementary information, Fig. 2D), witnessing a metabolic switch towards glycolysis. Thus, the metabolic shift observed in AB cells is clearly not related to the severity of CI deficiency but rather to the level of CI assembly defect.

Targeted inductions of CI assembly defects reproduce the metabolic impairment of AB cells

To reinforce the link between the CI assembly defect and the metabolic switch, we induced either a CI functional inhibition or a CI assembly defect in Ctr fibroblasts, using pharmacological agents or siRNA. First, piericidin A, a CI inhibitor that has no effect on its assembly (Fig. 3A1 and Supplementary information, Fig. 5A) was used to mimic the FA group. As expected, piericidin A significantly reduced the CI activity (-62±4%, Supplementary information, Fig. S5B) and all respiratory parameters (F, R and R-O respirations (- 53%, - 41% and - 72% compared to vehicle treated cells, Fig. 3A2), thus substantiating a decrease in the maximal respiratory chain capacity in accordance with the reduced CI enzymatic activity. However, the part of the respiratory capacity dedicated to the ATP synthesis was preserved ((R-O)/F, Fig. 3A3) thanks to a higher use of the maximal respiration capacity (R/F, Fig. 3A3). Piericidin A did not induce a glycolytic switch, as shown by a conserved metabolic orientation and L/G ratio (1.110 for vehicle *vs* 0.974 for piericidin A-treated cells, Fig. 3A4 and 3A5). Then, in order to induce the accumulation of CI assembly intermediates, we treated Ctr cells with either sodium pyrithione (NaPyr, Fig. 3B) or with a

siRNA targeting the assembly factor NDUFAF1 (Fig. 3C). NaPyr is a TIM23 modulator that favors the membrane sorting of nuclear-encoded respiratory chain complex subunits [28] and is thus expected to induce membrane intermediate accumulation. In NaPyr treated cells, a 60% increase of the membrane Pp-b intermediate together with a small decrease in CI holoenzyme quantity (-20% compared to vehicle, Figure 3B1 and Supplementary Figure 5A) were observed inducing a 46% decrease in R (routine) respiration and a 64% decrease in phosphorylationg (R-O) respiration without any significant modification of the respiratory complex activities (Supplementary Figure 5C). This leaded to a decrease in oxidative metabolism as evidenced by the 39% decrease in (R-O)/F ratio. NDUFAF1 is an assembly factor stabilizing the membrane Pp-b intermediate, thus its silencing by siRNA is expected to induce the accumulation of matrix Q intermediates. Inhibition of *NDUFAF1* expression (Supplementary information, Fig. S5D) decreased Pp-b intermediate amount, leading to a consistent accumulation of the Q/Pp-a intermediate (Fig. 3C1 and Supplementary information, Fig. S5A). Neither the accumulation of Pp-b (NaPyr treatment) nor of Q/Pp-a (*NDUFAF1* siRNA) intermediates significantly modified the maximal respiratory capacity (F, Fig. 3B2, 3C2). However, both the routine and phosphorylating respirations were decreased (R (-48% compared to vehicle treated cells) and R-O (-63% compared to vehicle treated cells), Fig. 3B2, 3C2), indicating an oxidative metabolism inhibition. Moreover, the accumulation of both Pp-b and Q/Pp-a intermediates decreased the part of the respiratory capacity used for ATP synthesis ((R-O)/F: -56% and -40%, respectively, Fig. 3B3, 3C3) and led to a higher conversion of glucose to lactate (L/G ratios: +77% and +39%, respectively, Fig. 3B4, 3C4). These results confirmed that CI disassembly slows down the oxidative metabolism and triggers a metabolic reprogramming towards glycolysis (Fig. 3B5, 3C5).

ROS overproduction due to CI misassembly is involved in the metabolic rewiring.

We previously demonstrated that CI assembly defect induced ROS overproduction linked to the presence of unconnected active N module [29]. In the present study, the presence of unassembled N module was evidenced by BN-PAGE in both control and mutated cells (Fig. 4A1), but did accumulate relative to CI holoenzyme quantity only in AB cells (Fig. 4A2). Maximal ROS production was measured in parallel to the maximal respiration rate, on permeabilized fibroblasts in the presence of CI and CI+CII (Fig. 4B) substrates. CI ROS production was somehow increased in the FA group (+54%), while drastically increased in the AB group (+421%). Furthermore, the ROS production increased with the NADH supply (St3 MPG *vs* St3 MP) in AB, but not in FA cells and remained higher than in Ctr cells even in the presence of the CII substrate (+100% for CI+CII, St3 MPGS, Fig. 4B). Regression analyses (Fig. 4C) indicated strong correlations between ROS production and both CI holoenzyme and unassembled N module quantities on one hand, and ROS production and metabolic orientation on the other hand. The ROS production by CI was also stimulated in NaPyr-treated cells (+60%, Fig. 4D), further emphasizing that CI disassembly is associated with increased ROS production. The cellular impact of ROS overproduction was assessed by measuring the lipid peroxidation adduct-content (4-hydroxynonenal, HNE) by Western blotting. HNE content was higher in AB than in FA and Ctr cells (+150%, Supplemental information, Fig. S6A1 and S6A2), revealing a systemic presence of oxidative stress specifically in the AB cells.

To further explore the involvement of ROS production in the metabolic switch, we induced in Ctr cells a CI-driven ROS overproduction using mito-Paraquat (mt-PQ) treatment [22]. mt-PQ treatment increased ROS production by 485% (Fig. 4E1) while inducing decrease in CI-linked respiration (-66%, Fig. 4E2) and CI maximal activity (-55%, Fig. 4E3). Additionally, mt-PQ

treatment reduced the routine (R, -55%, Fig. 4E4) and the phosphorylating respiration (R-O, -90%, Fig. 4E4), while it increased the L/G ratio (+38%, Fig. 4E5), thus emphasizing the onset of a glycolytic switch. Surprisingly, the treatment of Ctr cells with mt-PQ significantly reduced the amount of CI and II, with a particularly marked effect on the CI assembly (Fig. 4E6). Indeed, mt-PQ induced a drastic reduction in the amount of CI holoenzyme paralleled by the accumulation of an intermediate of about 700 kDa. This suggests a close interrelation between the levels of ROS production and CI assembly.

Alternatively, we inhibited ROS production with the anti-oxidant N-Acetyl Cysteine (NAC) [30, 31]. NAC treatment specifically increased both the routine (Routine, +50%) and the phosphorylating (R-O, +79%) respirations in AB cells (Fig. 4F1) and also significantly decreased the glucose conversion to lactate (L/G, -20%, Fig. 4F2). While NAC treatment increased CI holoenzyme quantity in Ctr cells, in AB cells, it did not alleviate the assembly defect of CI caused the mutations in nuclear-encoded CI subunit (Fig. 4F3 and supplemental information Fig. S6B1, B2). Despite a CI that remains disassembled, cellular metabolism returns to a more oxidative one with the antioxidant treatment (Fig. 4F1). This result indicates that the effects of NAC on cellular metabolism do indeed involve the decrease in ROS production and not a correction of the CI assembly defect in AB cells, placing ROS between the CI disassembly and the metabolic switch.

Altogether, these results emphasized that ROS overproduction is involved in a signaling pathway linking CI disassembly to the glycolytic switch.

A ROS/AMPK/PDH pathway is involved in the metabolic rewiring induced by CI disassembly

AMPK is a main sensor of mitochondrial energetic stress. In patient cells, AMPK phosphorylation was increased in AB group only (+74% compared to Ctr, Fig. 5A1). Interestingly, mt-PQ treatment of Ctr cells also induced an increase in AMPK phosphorylation (+ 71%, Fig. 5A2). Because the PDH-phosphorylation is an essential actor of the metabolic rewiring [32, 33] we monitored the phosphorylation status of the PDH E1α subunit. We found a 2.5-fold increase of its phosphorylation in the AB group, compared to the FA and control groups (Fig. 5B1). Furthermore, mt-PQ treatment enhanced the PDH phosphorylation in Ctr cells (+79%, Fig. 5B2). To decipher this signaling cascade, we inhibited either ROS production with NAC or AMPK activity using Compound C. Remarkably, both treatments decreased PDH phosphorylation in AB cells, with a higher extent for Compound C (-80%) than for NAC (-20%, Fig. 5C). Altogether, these results disclose a signaling pathway involving ROS overproduction due to CI disassembly, which induces the PDH over-phosphorylation in an AMPK dependent manner. To confirm the functional role of PDH inhibition in the decreased oxidative metabolism in AB cells, we assessed the mitochondrial pyruvate oxidation by measuring the formation of the tricarboxylic acid (TCA) cycle intermediates on permeabilized cells. In Ctr and FA cells, citrate and α-ketoglutarate were generated from pyruvate and malate oxidation (Fig. 5D) and only 5% of the pyruvate was converted to lactate. By contrast, in the AB group, pyruvate oxidation was strongly reduced and citrate formation was not detected, while a high level of lactate production was evidenced (+150%, Fig. 5D), confirming a blockage of pyruvate oxidation upstream of the TCA cycle, linked with the inhibition of the Pyruvate Dehydrogenase (PDH). We confirmed this observation by adding, during oxygraphic measurement, Glycerol-3-

Phosphate (G3P) which directly increases $FADH_2$ supply to the respiratory chain, bypassing the PDH regulation (Supplementary information, Fig. S7). G3P stimulated the oxidative metabolism, particularly in the AB group (+10%, +30% and +70%, in Ctr, FA and AB, respectively, Supplementary information, Fig. S7A1), with the routine respiration reaching the maximal capacity in the AB cells (R/F ratio close to 1, Supplementary information, Fig. S7A2) and led to a complete restoration of the part of the respiration dedicated to ATP synthesis ((R-O)/F, Supplementary information, Fig. S7A3). These results show that, in AB cells, the inhibition of mitochondrial pyruvate supply can be overcome by sustaining the $FADH_2$ production.

Our results, summarized in Fig. 6 A and B demonstrated that ROS overproduction was negatively correlated to CI assembly status and positively correlated to both PDH phosphorylation and metabolic rewiring placing this triad as a key determinant of the glycolytic switch.

DISCUSSION

Mitochondrial CI is the largest integral membrane enzyme of the respiratory chain. Its biogenesis is a highly intricate process involving the assembly of both nDNA- and MT-DNA-encoded proteins into subcomplex intermediates, finally combined into the functional holoenzyme. While defects in its assembly are a frequent cause of mitochondrial disorders, their relative contributions in the pathophysiology of CI-linked diseases have not been precisely studied. It has been shown that CI assembly is down-regulated under oxidative [34]

or hypoxic stress [35], and that unbalanced CI assembly causes premature senescence [19]. However, the effect of CI assembly defects and in particular the accumulation of assembly intermediates on cellular metabolism remains largely unknown.

In this study, we provide the first evidences demonstrating the central role of CI assembly, rather than CI activity, in the onset of the metabolic reprogramming in CI deficiency. Indeed, the glycolytic switch is not observed in cells with a pure CI catalytic defect, neither in patient cells nor in piericidin A-treated control cells. Moreover, the PCA-based statistical analysis clearly evidenced that the level of the metabolic switch is tightly correlated to the degree of CI disassembly. Our results suggest that rather than CI holoenzyme quantity, it is the accumulation of CI assembly intermediates that is involved in metabolic reprogramming. In this respect, a metabolic switch, evidenced by an increase in L/G ratio and a shutdown of oxidative metabolism ((R-O)/F) can be triggered by NaPyr treatment or NDUFAF1 downexpression in control cells by inducing a CI assembly intermediates overrepresentation, without impairing CI function. This further supports the fact that CI misassembly, but not its activity, is the culprit mechanism responsible for the metabolic switch and confirms a previous study suggesting that CI assembly could be involved in the switch of energy metabolism towards glycolysis, in smooth muscle cells in pulmonary hypertension [36].

This process occurs through a decrease in substrate inputs into the respiratory chain through the inhibition of the PDH and TCA cycle. CI not only acts as a metabolism hub essential to energy production but it is also one of the major source of ROS production [37]. In our study, although all the CI deficient cell lines displayed an increase in CI-related ROS production, the level of CI disassembly was the main contributor to ROS overproduction, a relationship already reported in Parkinson disease [38] and ageing [19]. We propose that this ROS overproduction is related to the toxicity of the CI intermediates, as we and others previously

demonstrated that, even when disconnected from the CI, the matrix N-module retains a NADH dehydrogenase activity [29, 39, 40] and participates to superoxide generation and oxidative stress [29]. Although known as damaging molecules, ROS are also increasingly considered as important signalling mediators [41, 42], notably involved in the AMPK dependent activation [43] of the PDH kinase [44] and glycolytic switch [45]. Here, we found that NAC antioxidant treatment partly reversed the PDH phosphorylation and the glycolytic switch, whereas increasing ROS production stimulated the AMPK and PDH phosphorylation and downstream the glycolytic metabolism. Our findings suggest that ROS production represents a tipping point, below which cells increase the catabolism to sustain the oxidative metabolism and over which cells shutdown the respiratory chain through PDH inhibition, impeding the metabolic flexibility necessary to meet the energetic cell requirements. Such a threshold of ROS overproduction is reached when a significant accumulation of CI assembly intermediates occurs. By contrast, in cells with a pure CI catalytic defect, a compensatory hyper-catabolism allows to maintain the oxidative metabolism at the expense of an increased fuel use. Ones can suppose that this hyper-catabolism copes with cellular metabolic requirements in basal conditions, but will fail to face an energetic challenge as exercise, infections or fasting.

Our conclusions demonstrating the importance of CI assembly in ROS production and in metabolic adaptations should prompt the improvement and refinement of antioxidant strategies and define targeted therapeutic routes for treating the two specific groups of CI patients that we defined in this work. Moreover, as CI deficiency is observed in an increasing number of pathophysiological situations as aging, cancer and neurological disorders, our data not only shed light on the importance of assessing CI assembly in these clinical conditions,

but also identified molecular pathways to be targeted for the design of future therapies of these diseases.

AUTHORS CONTRIBUTION

Conceptualization, methodology and writing - original draft: V.D.D., N.G.; validation: Ge.L, G.G; investigations: V.D.D., C.W., S.C., A.L., M.L.M., C.G., L.T., N.G.; resources: M.B., S.L., P.A.B., D.B.; data curation: D.G., writing-review and editing: M.S.K., S.K., A.C., V.P., P.R., G.L.; supervision: D.H., P.R., G.L.; funding acquisition: D.B., V.P., P.R., G.L.

ACKNOWLEDGMENTS

This work was supported by the following institutions and patient associations : Région Pays de la Loire, Angers Loire Métropole, Université d'Angers and CHU d'Angers, Fondation pour la Recherche Médicale, l'Union Nationale des Aveugles et Déficients Visuels, Retina France, Ouvrir les Yeux, Association contre les Maladies Mitochondriales, Fondation Maladies Rares. We are indebted to the partnership between the UNADEV and the ITMO NNP (l'Institut Thématique Multi-Organisme Neurosciences, sciences cognitives, neurologie, psychiatrie) / AVIESAN (alliance nationale pour les sciences de la vie et de la santé), for their involvement in research on diseases affecting the vision.

REFERENCES

[1] L. Iommarini, M.A. Calvaruso, I. Kurelac, G. Gasparre, A.M. Porcelli, Complex I impairment in mitochondrial diseases and cancer: parallel roads leading to different outcomes, Int J Biochem Cell Biol, 45 (2013) 47-63.

[2] L. Iommarini, I. Kurelac, M. Capristo, M.A. Calvaruso, V. Giorgio, C. Bergamini, A. Ghelli, P. Nanni, C. De Giovanni, V. Carelli, R. Fato, P.L. Lollini, M. Rugolo, G. Gasparre, A.M. Porcelli, Different mtDNA mutations modify tumor progression in dependence of the degree of respiratory complex I impairment, Hum Mol Genet, 23 (2014) 1453-1466.

[3] P. Peruzzo, M. Comelli, E. Di Giorgio, E. Franforte, I. Mavelli, C. Brancolini, Transformation by different oncogenes relies on specific metabolic adaptations, Cell Cycle, 15 (2016) 2656-2668.

[4] L.K. Sharma, H. Fang, J. Liu, R. Vartak, J. Deng, Y. Bai, Mitochondrial respiratory complex I dysfunction promotes tumorigenesis through ROS alteration and AKT activation, Hum Mol Genet, 20 (2011) 4605-4616.

[5] P. Wang, M. Song, Z.L. Zeng, C.F. Zhu, W.H. Lu, J. Yang, M.Z. Ma, A.M. Huang, Y. Hu, P. Huang, Identification of NDUFAF1 in mediating K-Ras induced mitochondrial dysfunction by a proteomic screening approach, Oncotarget, 6 (2015) 3947-3962.

[6] P. Jezek, L. Hlavata, Mitochondria in homeostasis of reactive oxygen species in cell, tissues, and organism, Int J Biochem Cell Biol, 37 (2005) 2478-2503.

[7] I.S. Kil, K.W. Ryu, S.K. Lee, J.Y. Kim, S.Y. Chu, J.H. Kim, S. Park, S.G. Rhee, Circadian Oscillation of Sulfiredoxin in the Mitochondria, Mol Cell, 59 (2015) 651-663.

[8] C. Canto, K.J. Menzies, J. Auwerx, NAD(+) Metabolism and the Control of Energy Homeostasis: A Balancing Act between Mitochondria and the Nucleus, Cell Metab, 22 (2015) 31-53.

[9] C. Canto, J. Auwerx, NAD+ as a signaling molecule modulating metabolism, Cold Spring Harb Symp Quant Biol, 76 (2011) 291-298.

[10] E.N. Maldonado, J.J. Lemasters, ATP/ADP ratio, the missed connection between mitochondria and the Warburg effect, Mitochondrion, 19 Pt A (2014) 78-84.

[11] E. Panieri, M.M. Santoro, ROS homeostasis and metabolism: a dangerous liason in cancer cells, Cell Death Dis, 7 (2016) e2253.

[12] L.R. Stein, S. Imai, The dynamic regulation of NAD metabolism in mitochondria, Trends Endocrinol Metab, 23 (2012) 420-428.

[13] R.J. Rodenburg, Mitochondrial complex I-linked disease, Biochim Biophys Acta, 1857 (2016) 938-945.
[14] G. Geffroy, R. Benyahia, S. Frey, V. Desquiret-Dumas, N. Gueguen, C. Bris, S. Belal, A. Inisan, A. Renaud, A. Chevrollier, D. Henrion, D. Bonneau, F. Letournel, G. Lenaers, P. Reynier, V. Procaccio, The accumulation of assembly intermediates of the mitochondrial complex I matrix arm is reduced by limiting glucose uptake in a neuronal-like model of MELAS syndrome, Biochim Biophys Acta, 1864 (2018) 1596-1608.
[15] K. Fiedorczuk, L.A. Sazanov, Mammalian Mitochondrial Complex I Structure and Disease-Causing Mutations, Trends Cell Biol, 28 (2018) 835-867.
[16] D. Ghezzi, M. Zeviani, Human diseases associated with defects in assembly of OXPHOS complexes, Essays Biochem, 62 (2018) 271-286.
[17] M. McKenzie, M.T. Ryan, Assembly factors of human mitochondrial complex I and their defects in disease, IUBMB Life, 62 (2010) 497-502.
[18] L. Sanchez-Caballero, S. Guerrero-Castillo, L. Nijtmans, Unraveling the complexity of mitochondrial complex I assembly: A dynamic process, Biochim Biophys Acta, 1857 (2016) 980-990.
[19] S. Miwa, H. Jow, K. Baty, A. Johnson, R. Czapiewski, G. Saretzki, A. Treumann, T. von Zglinicki, Low abundance of the matrix arm of complex I in mitochondria predicts longevity in mice, Nat Commun, 5 (2014) 3837.
[20] E. Hutter, K. Renner, G. Pfister, P. Stockl, P. Jansen-Durr, E. Gnaiger, Senescence-associated changes in respiration and oxidative phosphorylation in primary human fibroblasts, Biochem J, 380 (2004) 919-928.
[21] R. Fato, C. Bergamini, M. Bortolus, A.L. Maniero, S. Leoni, T. Ohnishi, G. Lenaz, Differential effects of mitochondrial Complex I inhibitors on production of reactive oxygen species, Biochim Biophys Acta, 1787 (2009) 384-392.
[22] E.L. Robb, J.M. Gawel, D. Aksentijevic, H.M. Cocheme, T.S. Stewart, M.M. Shchepinova, H. Qiang, T.A. Prime, T.P. Bright, A.M. James, M.J. Shattock, H.M. Senn, R.C. Hartley, M.P. Murphy, Selective superoxide generation within mitochondria by the targeted redox cycler MitoParaquat, Free Radic Biol Med, 89 (2015) 883-894.
[23] V. Desquiret-Dumas, N. Gueguen, G. Leman, S. Baron, V. Nivet-Antoine, S. Chupin, A. Chevrollier, E. Vessieres, A. Ayer, M. Ferre, D. Bonneau, D. Henrion, P. Reynier, V. Procaccio, Resveratrol induces a mitochondrial complex I-dependent increase in NADH

oxidation responsible for sirtuin activation in liver cells, J Biol Chem, 288 (2013) 36662-36675.
[24] F. Medja, S. Allouche, P. Frachon, C. Jardel, M. Malgat, B. Mousson de Camaret, A. Slama, J. Lunardi, J.P. Mazat, A. Lombes, Development and implementation of standardized respiratory chain spectrophotometric assays for clinical diagnosis, Mitochondrion, 9 (2009) 331-339.
[25] P. Benit, A. Slama, P. Rustin, Decylubiquinol impedes mitochondrial respiratory chain complex I activity, Mol Cell Biochem, 314 (2008) 45-50.
[26] M. Makrecka-Kuka, G. Krumschnabel, E. Gnaiger, High-Resolution Respirometry for Simultaneous Measurement of Oxygen and Hydrogen Peroxide Fluxes in Permeabilized Cells, Tissue Homogenate and Isolated Mitochondria, Biomolecules, 5 (2015) 1319-1338.
[27] V. Guillet, N. Gueguen, R. Cartoni, A. Chevrollier, V. Desquiret, C. Angebault, P. Amati-Bonneau, V. Procaccio, D. Bonneau, J.C. Martinou, P. Reynier, Bioenergetic defect associated with mKATP channel opening in a mouse model carrying a mitofusin 2 mutation, FASEB J, 25 (2011) 1618-1627.
[28] R.S. Aiyar, M. Bohnert, S. Duvezin-Caubet, C. Voisset, J. Gagneur, E.S. Fritsch, E. Couplan, K. von der Malsburg, C. Funaya, F. Soubigou, F. Courtin, S. Suresh, R. Kucharczyk, J. Evrard, C. Antony, R.P. St Onge, M. Blondel, J.P. di Rago, M. van der Laan, L.M. Steinmetz, Mitochondrial protein sorting as a therapeutic target for ATP synthase disorders, Nat Commun, 5 (2014) 5585.
[29] G. Leman, N. Gueguen, V. Desquiret-Dumas, M.S. Kane, C. Wettervald, S. Chupin, A. Chevrollier, A.S. Lebre, J.P. Bonnefont, M. Barth, P. Amati-Bonneau, C. Verny, D. Henrion, D. Bonneau, P. Reynier, V. Procaccio, Assembly defects induce oxidative stress in inherited mitochondrial complex I deficiency, Int J Biochem Cell Biol, 65 (2015) 91-103.
[30] O.I. Aruoma, B. Halliwell, B.M. Hoey, J. Butler, The antioxidant action of N-acetylcysteine: its reaction with hydrogen peroxide, hydroxyl radical, superoxide, and hypochlorous acid, Free Radic Biol Med, 6 (1989) 593-597.
[31] M. Benrahmoune, P. Therond, Z. Abedinzadeh, The reaction of superoxide radical with N-acetylcysteine, Free Radic Biol Med, 29 (2000) 775-782.
[32] T. Golias, I. Papandreou, R. Sun, B. Kumar, N.V. Brown, B.J. Swanson, R. Pai, D. Jaitin, Q.T. Le, T.N. Teknos, N.C. Denko, Hypoxic repression of pyruvate dehydrogenase activity is necessary for metabolic reprogramming and growth of model tumours, Sci Rep, 6 (2016) 31146.

[33] S. Zhang, M.W. Hulver, R.P. McMillan, M.A. Cline, E.R. Gilbert, The pivotal role of pyruvate dehydrogenase kinases in metabolic flexibility, Nutr Metab (Lond), 11 (2014) 10.
[34] K.R. Pryde, J.W. Taanman, A.H. Schapira, A LON-ClpP Proteolytic Axis Degrades Complex I to Extinguish ROS Production in Depolarized Mitochondria, Cell Rep, 17 (2016) 2522-2531.
[35] D.C. Fuhrmann, I. Wittig, S. Drose, T. Schmid, N. Dehne, B. Brune, Degradation of the mitochondrial complex I assembly factor TMEM126B under chronic hypoxia, Cell Mol Life Sci, 75 (2018) 3051-3067.
[36] R. Rafikov, X. Sun, O. Rafikova, M.L. Meadows, A.A. Desai, Z. Khalpey, J.X. Yuan, J.R. Fineman, S.M. Black, Complex I dysfunction underlies the glycolytic switch in pulmonary hypertensive smooth muscle cells, Redox Biol, 6 (2015) 278-286.
[37] J. Hirst, M.S. King, K.R. Pryde, The production of reactive oxygen species by complex I, Biochem Soc Trans, 36 (2008) 976-980.
[38] P.M. Keeney, J. Xie, R.A. Capaldi, J.P. Bennett, Jr., Parkinson's disease brain mitochondrial complex I has oxidatively damaged subunits and is functionally impaired and misassembled, J Neurosci, 26 (2006) 5256-5264.
[39] F. Valsecchi, C. Monge, M. Forkink, A.J. de Groof, G. Benard, R. Rossignol, H.G. Swarts, S.E. van Emst-de Vries, R.J. Rodenburg, M.A. Calvaruso, L.G. Nijtmans, B. Heeman, P. Roestenberg, B. Wieringa, J.A. Smeitink, W.J. Koopman, P.H. Willems, Metabolic consequences of NDUFS4 gene deletion in immortalized mouse embryonic fibroblasts, Biochim Biophys Acta, 1817 (2012) 1925-1936.
[40] J. Hirst, Energy transduction by respiratory complex I--an evaluation of current knowledge, Biochem Soc Trans, 33 (2005) 525-529.
[41] S.N. Jung, W.K. Yang, J. Kim, H.S. Kim, E.J. Kim, H. Yun, H. Park, S.S. Kim, W. Choe, I. Kang, J. Ha, Reactive oxygen species stabilize hypoxia-inducible factor-1 alpha protein and stimulate transcriptional activity via AMP-activated protein kinase in DU145 human prostate cancer cells, Carcinogenesis, 29 (2008) 713-721.
[42] L.B. Sullivan, N.S. Chandel, Mitochondrial reactive oxygen species and cancer, Cancer Metab, 2 (2014) 17.
[43] E.C. Hinchy, A.V. Gruszczyk, R. Willows, N. Navaratnam, A.R. Hall, G. Bates, T.P. Bright, T. Krieg, D. Carling, M.P. Murphy, Mitochondria-derived ROS activate AMP-activated protein kinase (AMPK) indirectly, J Biol Chem, (2018).

[44] C.A. Wu, Y. Chao, S.G. Shiah, W.W. Lin, Nutrient deprivation induces the Warburg effect through ROS/AMPK-dependent activation of pyruvate dehydrogenase kinase, Biochim Biophys Acta, 1833 (2013) 1147-1156.

[45] L. Plecita-Hlavata, J. Tauber, M. Li, H. Zhang, A.R. Flockton, S.S. Pullamsetti, P. Chelladurai, A. D'Alessandro, K.C. El Kasmi, P. Jezek, K.R. Stenmark, Constitutive Reprogramming of Fibroblast Mitochondrial Metabolism in Pulmonary Hypertension, Am J Respir Cell Mol Biol, 55 (2016) 47-57.

FIGURE LEGENDS:

Figure 1: Different metabolic orientations observed in CI deficient cells.

A. Cellular metabolic orientation, combined representation of the use of oxidative ((R-O)/F) and glycolytic (L/G ratio) capacities for each MT-ND, MT-TRNA and nDNA mutations. The results are expressed in percent of control cells. * indicates a significant difference (> +/- 2SD) compared to Ctr. **B. biplot of the PCA-X** (dot plots) **and loading plot of the explaining contribution of each metabolic parameter** (squares) **in the model.** CI maximal functions (CI/CS, st3 MP), maximal respiratory chain phosphorylating capacity (st3 MPS), maximal cellular oxidative capacity (FCCP: F), oxidative metabolism (Routine respiration: R), cellular phosphorylating respiration (R-O), relative cellular oxidative metabolism (R/F and R-O/F), glycolytic metabolism (L/G), parameters measured for each patient cell line were analyzed by a non-supervised multivariate process using the SIMCA software. The resulting model shows two components (cumulated R2X=0.722). The B group included most of the cells with nuclear mutated genes, the two MT-TL1 HL and the MT-TK cells. The A group encompassed all the MT-ND mutated cells, the MT-TL LL and the MT-TP cells, and the three nuclear mutated NDUFA9, NDUFS4.1 and NDUFV1.1 cells. **C1. Orthogonal Projections to Latent Structures Discriminant Analysis (OPLS-DA) analysis of the two patient groups A and B,** determined in the PCA analysis. **C2. Corresponding Volcano plot.** In the "Volcano" plot, the x-axis represents the coefficient of the regression between the X (analyzed parameters) and Y (response) matrix, while the variable importance for the projection (VIP) is represented on the y-axis. The VIP summarizes the importance of each variable in defining both the X matrix and the correlation between X and Y. Variables with a VIP value ≥ 1 are considered as pertinent for the model. **D. Oxidative metabolism** was analysed on intact cells in glucose medium by measuring the: **D1. Routine respiration,**

corresponding to the cellular respiration rate, **D2. Phosphorylating respiration (R-O),** determined after ATP synthesis inhibition by oligomycin**. D3. Use of the spare capacity for phosphorylation ((R-O)/F),** *i.e.* part of the maximal respiratory capacity used to sustain oxidative phosphorylation (R-O). **E. Glycolytic metabolism. E1. Cellular Glucose consumption and Lactate production,** measured in culture media. **E2. Use of the glycolytic capacity,** determined by the conversion rate of the glucose (G) to lactate (L) (L/G ratio). **F. Cellular ATP/ADP ratio** measured with or without oligomycin (Oligo, 4µg/ml) to inhibit mitochondrial ATP synthesis**. G. Cellular metabolic orientation,** determined by the ratio between the glucose to lactate fueling (G to L) and the use of oxidative capacity ((R-O)/F). **H1. CI activity,** normalized to the CS one. **H2. CI-linked maximal respiration** in coupling conditions with malate, pyruvate (St3 MP).. **I1. Correlation between the metabolic orientation and the CI /CS ratio. I2. Correlation between the metabolic orientation and the CI-linked maximal respiration (St3 MP). J. Cellular NAD+/NADH ratio** determined on fresh cell lysates from Ctr and patient fibroblasts. **K. Correlation between the metabolic orientation and cellular NAD+/NADH ratio.**

A, D1, D2, D3, E1, E2, F, G, H1, H2, J: Analyses were performed at least on two biological replicate for each cell lines of each group. Results are presented as means ± SEM. * indicates a significant difference compared with Ctr group and § a significant difference among patient groups (A *vs* B). I1, I2 and K: statistical significance of correlations was evaluated by the *F* test using Sigma Plot Software.

Figure 2: Induction of CI disassembly, but not CI deficiency, triggers a metabolic shift

A. CI assembly analysis. A1. In the first immunoblot, CI holoenzyme level was analyzed by sequential hybridization of NDUFB6+NDUFS2 and SDHA antibodies. A2. The assembly intermediates were detected in parallel on the same samples but different immunoblots by sequential hybridization with anti-NDUFAF4, NDUFAF1, NDUFAF2, specifically targeting different assembly intermediates (see Supplementary Figure 1), and SDHA or. Analyses were performed at least in two biological replicates for each cell lines of each group. **B1. Left panel. CI holoenzyme quantity**. The CI holoenzyme quantity was normalized to the CII one and is represented as a mean ± *SEM* for each group. **Right panel. Assembly intermediates**. The total Assembly Intermediate (A.I.) quantity was normalized to the CII one and is represented as a mean ± *SEM* for each group. **B2. Accumulation of assembly intermediates relative to CI holoenzyme quantity. C. Correlation between the metabolic orientation and CI assembly. D. Analysis of : Cellular metabolic orientation** determined by the ratio between the use of glycolytic capacity (L/G) and the use of oxidative capacity ((R-O)/F) in the four FA cells and three AB cells (upper left panel) displaying different **CI assembly profiles** (upper right panel) but comparable CI functions **(maximal CI activity (I/CS) and CI-linked respiration (**St3 MP, lower left panel)) and **maximal respiratory chain capacity**, either in coupled state (permeabilized cell, St3 MPS) or in uncoupled state (intact cells, FCCP, lower right panel). The blue bars represent the Ctr values. § indicates a significant difference between FA cells and AB ones.

B1, B2: Analyses were performed at least in two biological replicates for each cell lines of each group. Results are presented as means ± SEM. * indicates a significant difference compared with Ctr group and § a significant difference among patient groups (FA *vs* AB). C: statistical significance of correlations was evaluated by the *F* test. Ctr, n=11; Group A, n=19; Group B, n=10.

Figure 3: Pharmacologically-induced CI disassembly but not CI deficiency induced metabolic rewiring in Ctr fibroblasts.

A, B, C. Effect of induced CI deficiency (A) or disassembly (B, C) on Ctr fibroblasts using either **A. Piericidin A** (5 nM) *vs* DMSO (1:5,000), **B. sodium pyrithione** (NaPyr, 1µM) *vs* DMSO (1:5,000) or **C. transfection with *NDUFAF1* or Scramble siRNA,** for 48H in each condition. **A1, B1, C1. Quantification of CI holoenzyme and assembly intermediates.** Relative amounts of CI holoenzyme and assembly intermediates from treated fibroblasts are normalized to CII and expressed relative to the vehicle / scramble conditions. **A2, B2, C2 Maximal cellular oxidative capacity** (F), and **Oxidative metabolism**, i.e. Routine respiration (R) and phosphorylating respiration (R-O) determined on Ctr and treated fibroblasts. **A3, B3, C3. Metabolic compensations,** i.e. use of the maximal capacity to sustain cellular oxidative phosphorylation ((R-O)/F) or oxidative metabolism (R/F). **A4, B4, C4. Glycolytic metabolism,** determined by the conversion rate of the glucose to lactate (L/G ratio) measured in culture media. **A5, B5, C5. Cellular metabolic orientation,** represented the use of oxidative ((R-O)/F) and glycolytic (L/G ratio) capacities of cells**.** Results are expressed relative to the vehicle / scramble conditions and represented as a mean ± *SEM*. n=3 independent experiments for each treatment. # indicates a significant difference compared to vehicle or scramble.

Figure 4: ROS overproduction is involved in metabolic reprogramming

A. Analysis of free N module accumulation in Ctr and patient cells**.** After BN-PAGE, free N module and fully assembled CI (bound N module) were detected using anti-NDUFS1 antibody. **A1. Representative blots** of one of the duplicate experiments**.** The different groups

are highlighted by different colors: the Ctr cells are in blue, FA cells are in red and AB cells in green. **A2. Quantification of free N module relative to fully assembled CI (bound N module)** in 10 Ctr, 14 FA and 10 AB cell lines**. B. ROS production** measured by fluorescence detection of Amplex Red oxidation on permeabilized fibroblasts. Dedicated CI and CI+CII-linked ROS production was sequentially analysed using substrates of CI and CI+CII as followed: first, NADH supply to CI was induced by adding pyruvate and malate (MP) in the presence of saturating ADP concentration. Then, NADH supply was further increased by addition of glutamate (MPG). Finally, Succinate (MPGS) was added to measure the ROS production with convergent CI+II electron flow into the Q-junction. ROS production was normalized to the corresponding oxygen consumption measured in parallel in the same oxygraphic chambers (n=5 for Ctr, n=9 for FA and n=9 for AB). Results are represented as a mean ± *SEM*. * indicates a significant difference with Ctr and § with the FA groups. **C. Correlation between the CI-linked ROS production and the relative unbound N module** (upper left panel)**, the cellular metabolic orientation** (upper right panel) **and the CI quantity** (lower left panel)**. D. ROS production analysis in NaPyr and vehicle-treated cells** successively respiring with CI substrates (pyruvate + malate, pyruvate + malate + glutamate) and CI+CII substrates (pyruvate + malate + glutamate + succinate). # indicates a significant effect of NaPyr addition. **E. Effect of mt-PQ treatment on cell metabolism and CI assembly in Ctr and AB cells. E1. ROS production analysis** with CI substrates (malate, pyruvate, glutamate). ROS overproduction was induced in Ctr fibroblast by mito-Paraquat (mt-PQ) treatment (5 µM, 48H). **E2. Maximal coupled CI-linked respiration (**malate, pyruvate, glutamate, St3 MPG) after mt-PQ treatment. **E3. Maximal CI activity** normalized to CS one after mt-PQ treatment. **E4. Routine respiration** (R) **and phosphorylating respiration** (R-O). **E5. Glycolytic metabolism** i.e. the ratio of the lactate production to glucose consumption measured in culture media (L/G) determined on Ctr and mt-PQ treated

fibroblasts. n=3 different Ctr cell lines, analysed in two biological replicates. Results are represented as a mean ± *SEM*. * indicates a significant difference with Ctr and # indicates a significant effect of mt-PQ. **E6. Blue Native PAGE analysis of DMSO and mtPQ treated cells.** Left panel: representative Blue Native PAGE gel; Right panel: Quantification of CI holoenzyme (CI), assembly intermediates (AI) and respiratory chain complexes (CI, CII, CIII et CIV) after DMSO or mtPQ incubation in Ctr cells n=3 in duplicate. Results are represented as a mean ± *SEM*. # indicates a significant effect of mt-PQ ($p<0.05$). **F. Effect of NAC treatment on cell metabolism and CI assembly in Ctr and AB cells. F1. Oxidative metabolism** in Ctr and AB cells treated with the antioxidant N-Acetyl Cysteine (NAC, 1 mM, 48H) **Left, Routine respiration** (R, left panel) and **Right, Phosphorylating respiration** (R-O, right panel). **F2. Glycolytic metabolism,** determined by the conversion rate of the glucose to lactate (L/G ratio) measured in culture media. **F3. CI assembly analysis.** Left panel: representative Blue Native PAGE gel sequentially hybridized with NDUFS2+NDUFB6 and SDHA; Right panel: Quantification of CI holoenzyme (CI). Experiments were performed on 4 different Ctr cell lines (3 different Ctr cell lines for BN-PAGE experiments), and 5 different AB cell lines, using representative cell lines with different assembly defects, i.e. MT-TL1.3, NDUFV1.2, NDUFS4.3, NDUFB3 and NDUFS7. Results are represented as a mean ± *SEM*. # indicates a significant effect of the treatment. * indicates a significant difference with Ctr cells in the same conditions.

Figure 5: ROS/AMPK pathway is involved in limitation of substrate supply to respiratory chain by inhibition of PDH in AB cells.

A1. AMPK phosphorylation level analyzed by Western blotting in cell lysates. Left panel: representative blot, right panel: quantitation of P-AMPK (in green) relative to total AMPK (in

red). Each cell line was analyzed in two biological replicates, Ctr: n=10, FA: n=14 and AB: n=9. Results are represented as a mean ± *SEM.* * indicates a significant difference with Ctr. **A2. Effect of ROS overproduction on AMPK phosphorylation.** Left panel: representative blot of Ctr cells treated with Vehicle (DMSO 1:5000) or mt-PQ, right panel: quantitation of P-AMPK (in green) relative to total AMPK (in red). Western blots realized on n=3 Ctr in duplicate, # indicates a significant effect of the treatment. **B1. PDH phosphorylation level** analyzed by Western blotting in cell lysates. Left panel. Representative blots. Phospho-PDH, in red and total PDH, in green. Right panel. Quantitation of P-PDH relative to total PDH. Each cell line was analyzed in two biological replicates, Ctr: n=6, FA: n=10 and AB: n=9. Results are represented as a mean ± *SEM.* * indicates a significant difference with Ctr. **B2. Effect of ROS overproduction on PDH phosphorylation.** representative blot of P-PDH (in red) and total PDH (in green) in Ctr cells treated with Vehicle (DMSO 1:5000) or mt-PQ and quantitation of P-PDH relative to total PDH expressed in percent of Veh treated cells. Western blots realized on n=3 Ctr in duplicate, # indicates a significant effect of the treatment. **C. Effect of inhibition of ROS production and of AMPK on PDH phosphorylation.** Left panel: Representative blots of PDH phosphorylation level analyzed by Western blotting in cell lysates**.** Phospho-PDH, in red and total PDH, in green. Right panel: quantitation of P-PDH relative to total PDH. Experiments were performed on 4 different Ctr cell lines and 5 different AB cell lines, using representative cell lines with different assembly defects, i.e. MT-TL1.3, NDUFV1.2, NDUFS4.3, NDUFB3 and NDUFS7. Results are represented as a mean ± *SEM.* # indicates a significant effect of the treatment. **D. Analysis of pyruvate metabolism and TCA cycle functioning.** Oxidation of pyruvate and malate was followed on permeabilized fibroblasts from Ctr (n=4), FA (n=7), and AB (n=7) groups. Malate, the oxaloacetate precursor, was added with pyruvate to support full TCA cycling and respiration was induced by sub-saturating ADP concentration (0.5mM, 60% of *V*max) to

mimic the phosphorylating respiration observed in intact cells. NAD+ was omitted to preserve an eventual allosteric regulation of PDH and/or TCA cycle.

Figure 6: Sum up of the discriminative parameters of metabolic adaptations induced by CI deficiency

Principal Component Analysis (PCA-X) of the cohort of CI deficient patients. A1: biplot of the PCA-X (dot plots) and loading plot of the explaining contribution of each metabolic parameter (squares) in the model. CI maximal activity (CI/CS, st3 MP), maximal respiratory chain phosphorylating capacity (st3 MPS), maximal cellular oxidative capacity (FCCP: F), oxidative metabolism (Routine respiration: R), cellular phosphorylating respiration (R-O), relative cellular oxidative metabolism (R/F and R-O/F), glycolytic metabolism (L/G), AMPK phosphorylation, ADP/ATP ratio, NAD+/NADH ratio and CI assembly (CI holoenzyme quantity: CI and Assembly Intermediates, A.I.) parameters were measured for each control (Ctr) and patient cell line and analyzed by a non-supervised multivariate process using the SIMCA software (R^2X(Cum)=0.661 and Q^2=0.423. **A2. Volcano plot of the orthogonal Projections to Latent Structures Discriminant Analysis (OPLS-DA,** (R^2X(Cum)=0.637 and Q^2=0.86**) analysis of patient cell lines.** In the "Volcano" plot, the x-axis represents the coefficient of the regression between the X (analyzed parameters) and Y (response) matrix, while the variable importance for the projection (VIP) is represented on the y-axis. The VIP summarizes the importance of each variable in defining both the X matrix and the correlation between X and Y. Variables with a VIP value ≥1 are considered as pertinent for the model. **B. Correlation matrix of the PCA model** obtained from the cell cohort (patient cells, n=29) for all biochemical parameters. I/CS: maximal CI activity (NADH Ubiquinone Reductase) reported to that of citrate synthase (CS). St3 MP:

maximal CI-linked phosphorylating respiration measured on permeabilized cells. St3 MPS: maximal CI+CII-linked phosphorylating respiration measured on permeabilized cells, i.e. maximal OXPHOS capacity. F: maximal uncoupled respiration measured on intact cell respiring in glucose medium, i.e. maximal cellular oxidative capacity. R: Routine respiration measured on intact cell, i.e. oxidative metabolism, R-O: Phosphorylating respiration measured on intact cell as the oligomycin-sensitive respiration, R-O/F: part of the spare respiratory chain capacity used for ATP synthesis, R/F: part of the spare respiratory chain capacity to sustain respiration, L/G: glycolytic metabolism estimated by the Lactate/Glucose ratio, P-PDH : phosphorylation status of the PDH, CI: quantity of CI holoenzyme, A.I.: quantity of CI assembly intermediates, N/CI: quantification of the accumulation of free N module compared with CI holoenzyme, ROS: ROS production per oxygen consumed in presence of CI substrates, NAD: cellular NAD+/NADH ratio, ATP/ADP: cellular ATP/ADP ratio, P-AMPK : AMPK phosphorylation status.

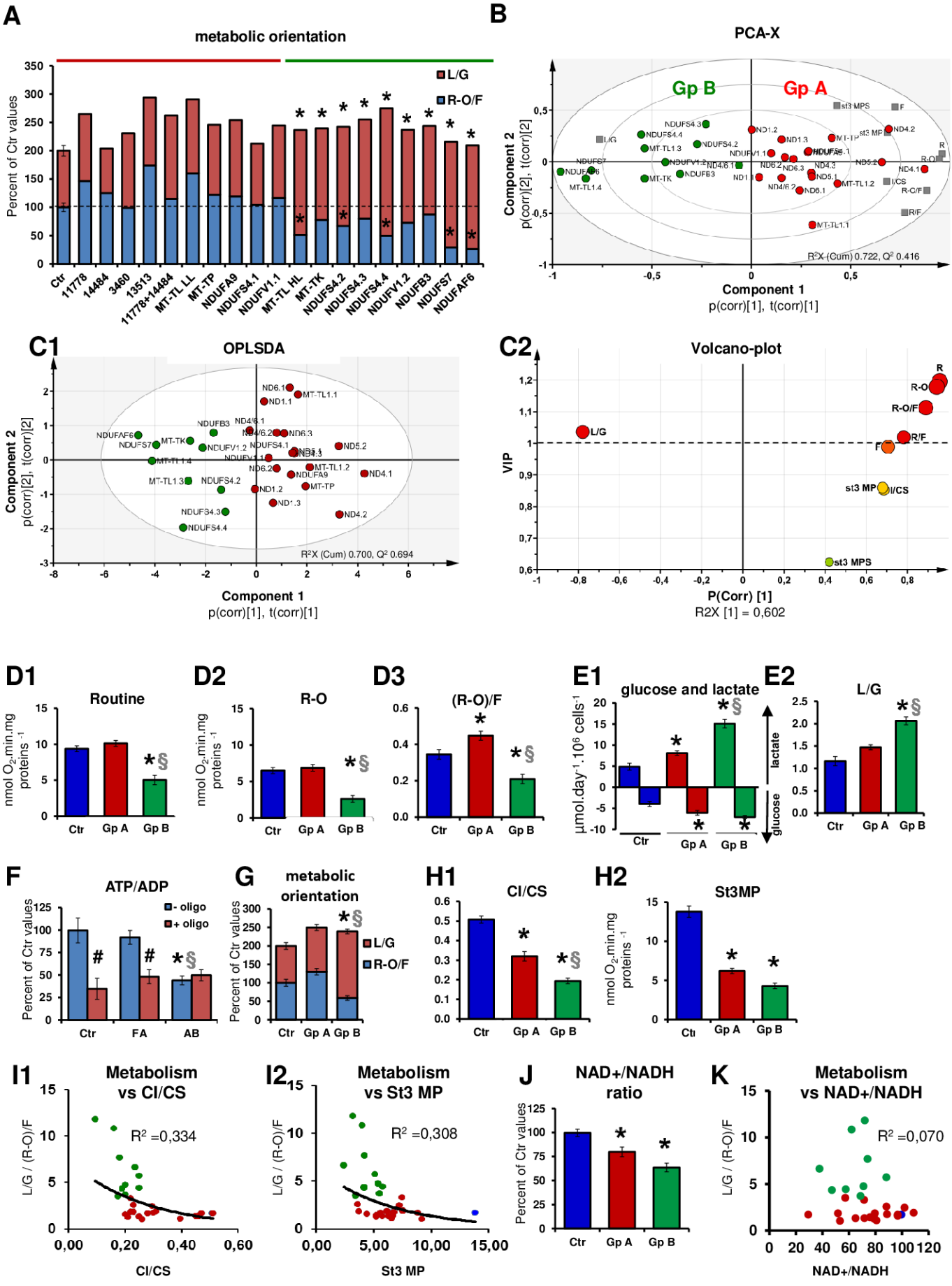
A
metabolic orientation
L/G
R-O/F
Percent of Ctr values
Ctr
11778
14484
3460
13513
11778+14484
MT-TL LL
MT-TP
NDUFA9
NDUFS4.1
NDUFV1.1
MT-TL HL
MT-TK
NDUFS4.2
NDUFS4.3
NDUFS4.4
NDUFV1.2
NDUFB3
NDUFS7
NDUFAF6
B
PCA-X
Gp B
Gp A
Component 2
p(corr)[2], t(corr)[2]
Component 1
p(corr)[1], t(corr)[1]
R²X (Cum) 0.722, Q² 0.416
C1
OPLSDA
Component 2
p(corr)[2], t(corr)[2]
Component 1
p(corr)[1], t(corr)[1]
R²X (Cum) 0.700, Q² 0.694
C2
Volcano-plot
VIP
P(Corr) [1]
R2X [1] = 0,602
D1
Routine
nmol O2.min.mg proteins -1
D2
R-O
D3
(R-O)/F
E1
glucose and lactate
µmol.day-1.10⁶ cells-1
lactate
glucose
E2
L/G
F
ATP/ADP
- oligo
+ oligo
Percent of Ctr values
Ctr
FA
AB
G
metabolic orientation
L/G
R-O/F
H1
CI/CS
H2
St3MP
I1
Metabolism vs CI/CS
R² =0,334
L/G / (R-O)/F
CI/CS
I2
Metabolism vs St3 MP
R² =0,308
St3 MP
J
NAD+/NADH ratio
K
Metabolism vs NAD+/NADH
R² =0,070
NAD+/NADH
Ctr
Gp A
Gp B

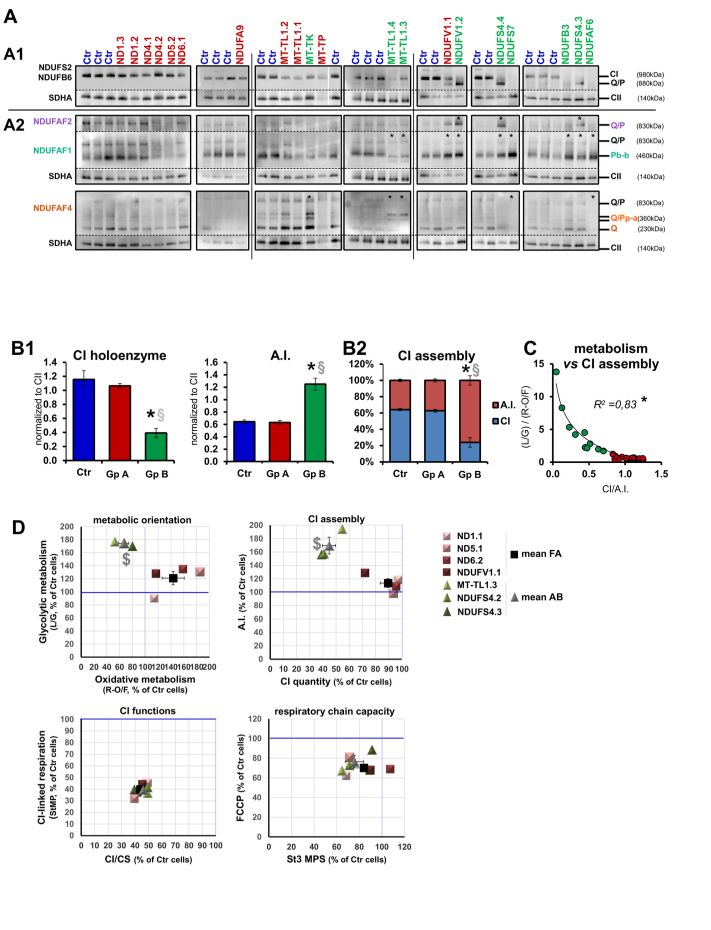
A
A1
NDUFS2
NDUFB6
SDHA
Ctr
ND1.3
ND1.2
ND4.1
ND4.2
ND5.2
ND6.1
NDUFA9
MT-TL1.2
MT-TL1.1
MT-TK
MT-TP
MT-TL1.4
MT-TL1.3
NDUFV1.1
NDUFV1.2
NDUFS4.4
NDUFS7
NDUFB3
NDUFS4.3
NDUFAF6
CI (980kDa)
Q/P (880kDa)
CII (140kDa)
A2
NDUFAF2
NDUFAF1
NDUFAF4
Q/P (830kDa)
Pb-b (460kDa)
Q/Pp-a (360kDa)
Q (230kDa)
B1
CI holoenzyme
normalized to CII
Ctr
Gp A
Gp B
A.I.
B2
CI assembly
A.I.
CI
C
metabolism
vs CI assembly
(L/G) / (R-O/F)
R² =0,83
CI/A.I.
D
metabolic orientation
Glycolytic metabolism
(L/G, % of Ctr cells)
Oxidative metabolism
(R-O/F, % of Ctr cells)
CI assembly
A.I. (% of Ctr cells)
CI quantity (% of Ctr cells)
ND1.1
ND5.1
ND6.2
NDUFV1.1
MT-TL1.3
NDUFS4.2
NDUFS4.3
mean FA
mean AB
CI functions
CI-linked respiration
(SMP, % of Ctr cells)
CI/CS (% of Ctr cells)
respiratory chain capacity
FCCP (% of Ctr cells)
St3 MPS (% of Ctr cells)

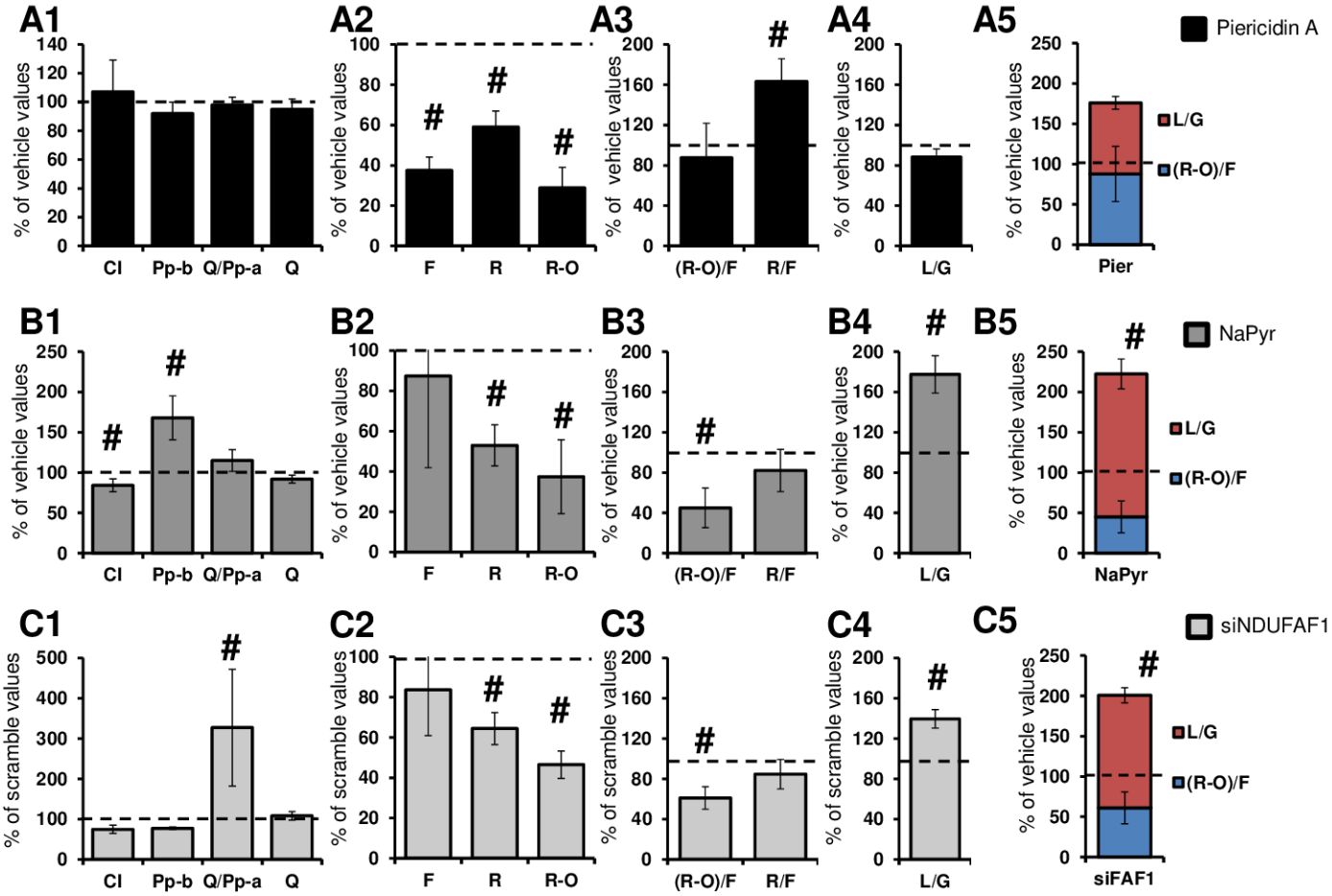
A1
A2
A3
A4
A5
Piericidin A
% of vehicle values
CI
Pp-b
Q/Pp-a
Q
F
R
R-O
(R-O)/F
R/F
L/G
Pier
B1
B2
B3
B4
B5
NaPyr
C1
C2
C3
C4
C5
siNDUFAF1
% of scramble values
siFAF1
#

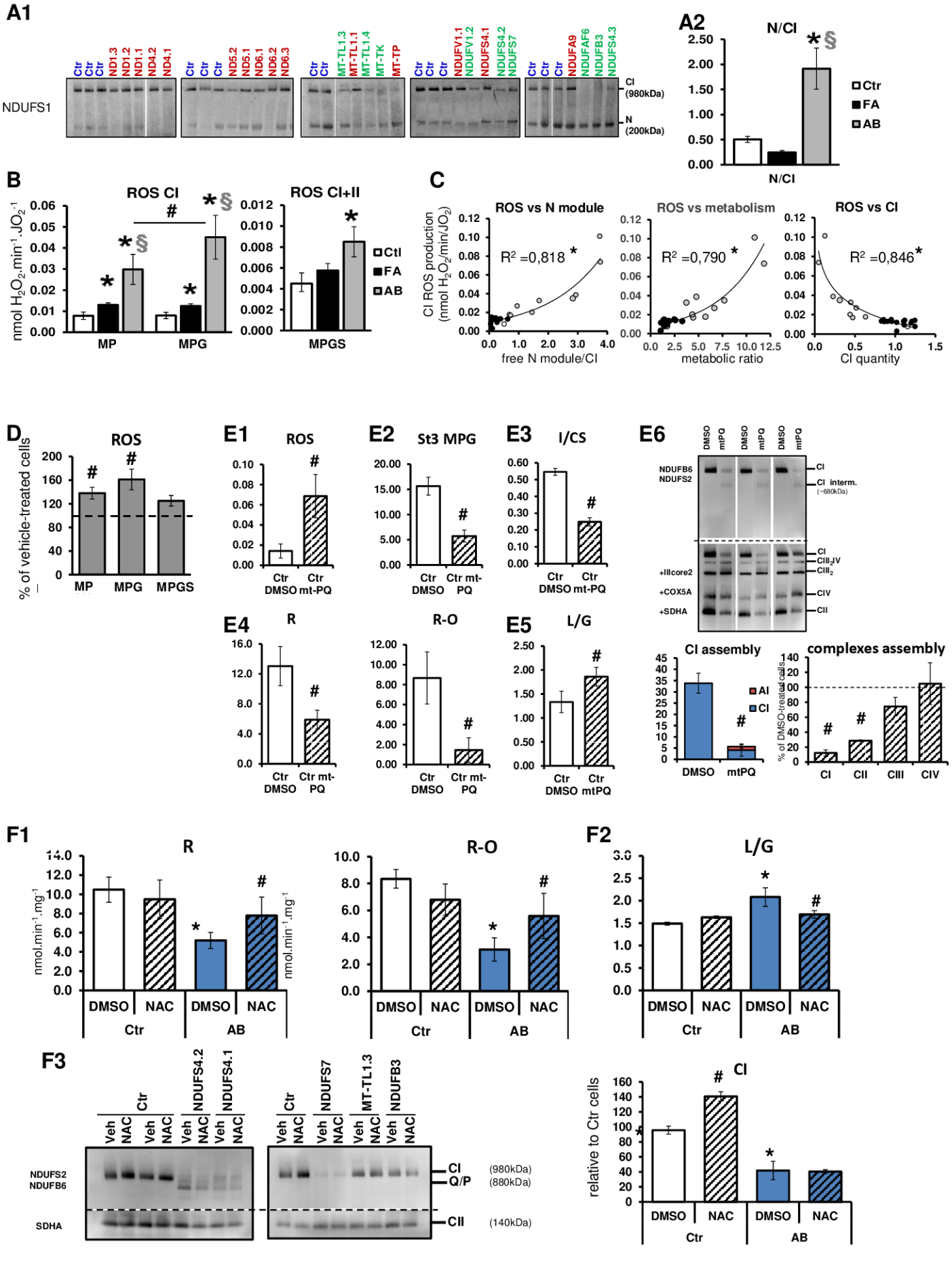
A1
NDUFS1
Ctr Ctr Ctr ND1.3 ND1.2 ND1.1 ND4.2 ND4.1
Ctr Ctr Ctr ND5.2 ND5.1 ND6.1 ND6.2 ND6.3
Ctr Ctr MT-TL1.3 MT-TL1.1 MT-TL1.4 MT-TK MT-TP
Ctr Ctr Ctr NDUFV1.1 NDUFV1.2 NDUFS4.1 NDUFS4.2 NDUFS7
Ctr Ctr Ctr NDUFA9 NDUFAF6 NDUFB3 NDUFS4.3
CI (980kDa)
N (200kDa)
A2
N/CI
Ctr
FA
AB
B
ROS CI
ROS CI+II
nmol H2O2.min-1.JO2-1
MP
MPG
MPGS
Ctl
FA
AB
C
ROS vs N module
ROS vs metabolism
ROS vs CI
CI ROS production (nmol H2O2/min/JO2)
R2 =0,818 *
R2 =0,790 *
R2 =0,846*
free N module/CI
metabolic ratio
CI quantity
D
ROS
% of vehicle-treated cells
MP
MPG
MPGS
E1
ROS
E2
St3 MPG
E3
I/CS
Ctr DMSO
Ctr mt-PQ
E4
R
E5
L/G
R-O
Ctr mtPQ
E6
DMSO
mtPQ
NDUFB6
NDUFS2
CI
CI interm. (~680kDa)
+IIIcore2
+COX5A
+SDHA
CIII2IV
CIII2
CIV
CII
CI assembly
AI
CI
complexes assembly
% of DMSO-treated cells
CII
CIII
F1
R
R-O
nmol.min-1.mg-1
DMSO
NAC
Ctr
AB
F2
L/G
F3
Veh
NAC
NDUFS4.2
NDUFS4.1
NDUFS7
MT-TL1.3
NDUFB3
NDUFS2
NDUFB6
SDHA
CI
Q/P
CII
(980kDa)
(880kDa)
(140kDa)
relative to Ctr cells

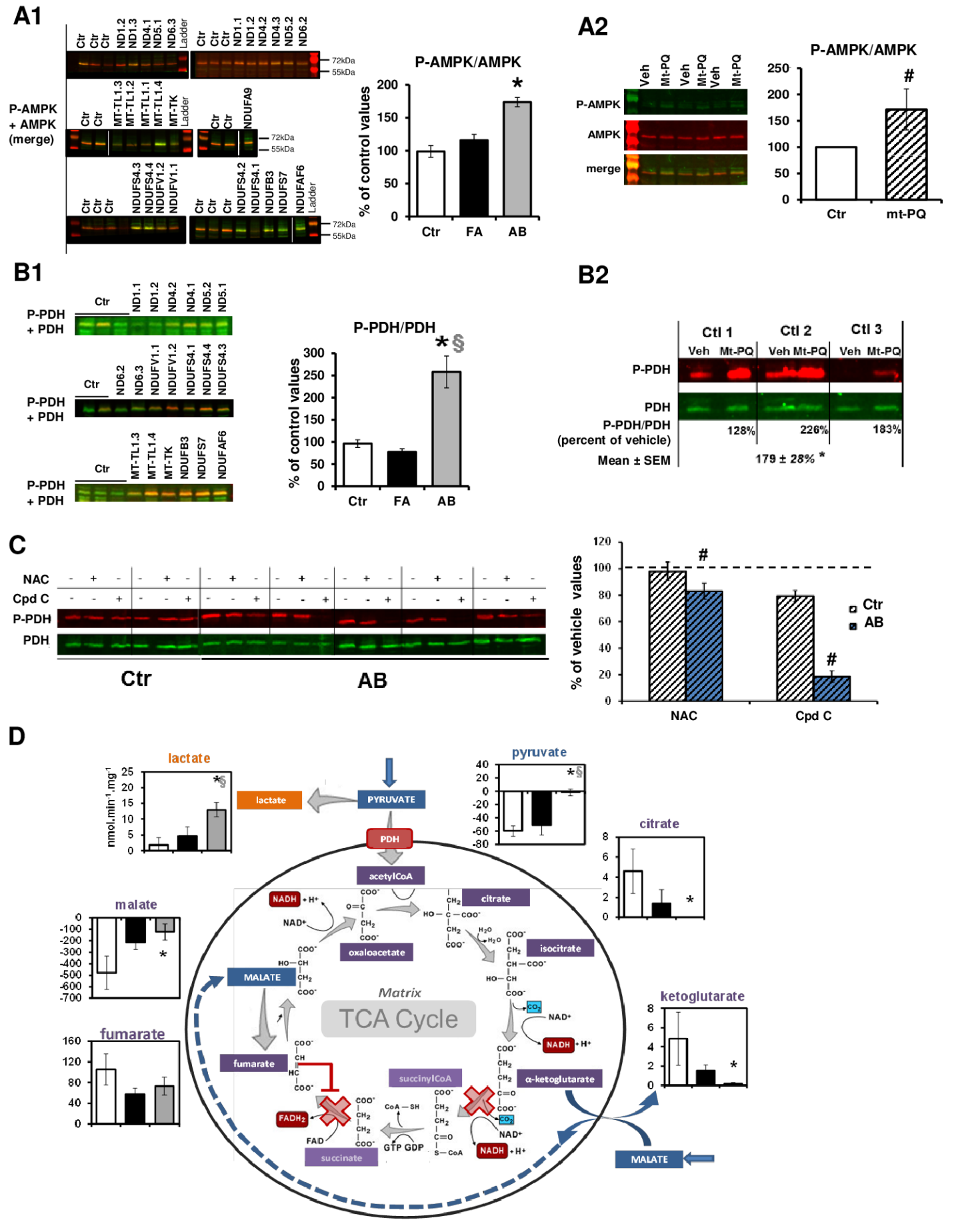
A1
P-AMPK + AMPK (merge)
Ctr Ctr Ctr ND1.2 ND1.3 ND4.1 ND5.1 ND6.3 Ladder
Ctr Ctr ND1.1 ND1.2 ND4.2 ND4.3 ND5.2 ND6.2
Ctr Ctr MT-TL1.3 MT-TL1.2 MT-TL1.1 MT-TL1.4 MT-TK Ladder
Ctr Ctr NDUFA9
Ctr Ctr Ctr NDUFS4.3 NDUFS4.4 NDUFV1.2 NDUFV1.1
Ctr Ctr NDUFS4.2 NDUFS4.1 NDUFB3 NDUFS7 NDUFAF6 Ladder
72kDa
55kDa
P-AMPK/AMPK
% of control values
Ctr FA AB
A2
Veh Mt-PQ Veh Mt-PQ Veh Mt-PQ
P-AMPK
AMPK
merge
P-AMPK/AMPK
Ctr mt-PQ
B1
P-PDH + PDH
Ctr ND1.1 ND1.2 ND4.2 ND4.1 ND5.2 ND5.1
Ctr ND6.2 ND6.3 NDUFV1.1 NDUFV1.2 NDUFS4.1 NDUFS4.4 NDUFS4.3
Ctr MT-TL1.3 MT-TL1.4 MT-TK NDUFB3 NDUFS7 NDUFAF6
P-PDH/PDH
% of control values
Ctr FA AB
B2
Ctl 1 Ctl 2 Ctl 3
Veh Mt-PQ Veh Mt-PQ Veh Mt-PQ
P-PDH
PDH
P-PDH/PDH (percent of vehicle)
128% 226% 183%
Mean ± SEM
179 ± 28% *
C
NAC
Cpd C
P-PDH
PDH
Ctr
AB
% of vehicle values
NAC Cpd C
Ctr
AB
D
lactate
pyruvate
citrate
malate
fumarate
ketoglutarate
nmol.min-1.mg-1
PYRUVATE
PDH
acetylCoA
citrate
isocitrate
α-ketoglutarate
succinylCoA
succinate
fumarate
MALATE
oxaloacetate
Matrix
TCA Cycle
NADH + H+
NAD+
FADH2
FAD
GTP GDP
CoA — SH
CO2
H2O

A1

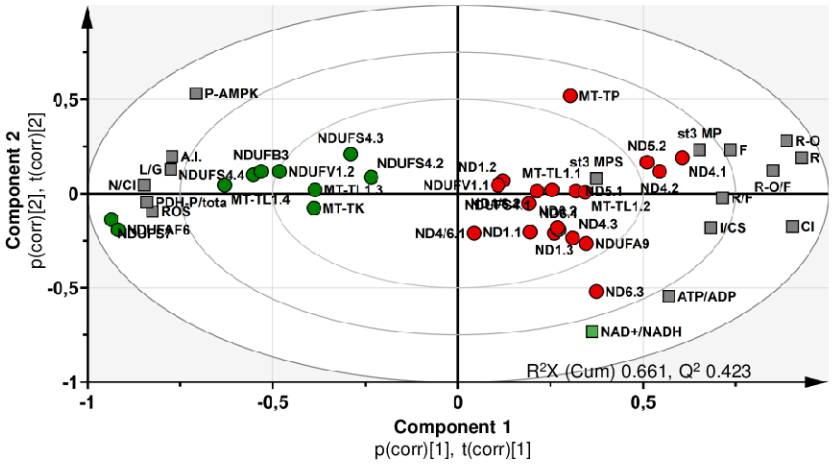

A2

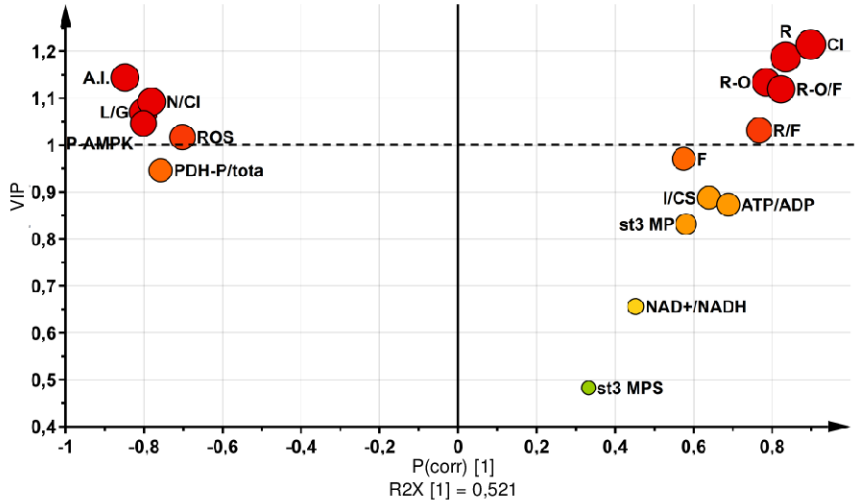

B

	I/CS	st3 MP	st3 MPS	F	R	R-O	R-O/F	R/F	L/G	NADH	CI	A.I.	ROS	N/CI	ATP/ADP	P-PDH	P-AMPK
I/CS	1.000	0.408	0.075	0.483	0.589	0.569	0.495	0.466	-0.607	0.395	0.567	-0.586	-0.536	-0.556	0.180	-0.501	-0.490
st3 MP		1.000	0.280	0.579	0.616	0.574	0.460	0.371	-0.603	0.095	0.424	-0.511	-0.512	-0.451	0.436	-0.572	-0.521
st3 MPS			1.000	0.353	0.410	0.405	0.321	0.250	-0.224	0.246	0.272	-0.222	-0.216	-0.145	0.392	-0.410	-0.059
F				1.000	0.816	0.743	0.456	0.197	-0.411	0.277	0.676	-0.476	-0.688	-0.645	0.230	-0.647	-0.409
R					1.000	0.956	0.827	0.701	-0.602	0.243	0.783	-0.694	-0.724	-0.712	0.406	-0.736	-0.558
R-O						1.000	0.853	0.699	-0.616	0.117	0.721	-0.647	-0.670	-0.681	0.440	-0.686	-0.467
R-O/F							1.000	0.872	-0.640	0.174	0.693	-0.639	-0.671	-0.653	0.486	-0.721	-0.482
R/F								1.000	-0.581	0.181	0.559	-0.663	-0.422	-0.443	0.404	-0.511	-0.479
L/G									1.000	-0.236	-0.701	0.610	0.592	0.600	-0.592	0.569	0.553
NAD+/NADH										1.000	0.380	-0.392	-0.216	-0.217	0.331	-0.321	-0.479
CI											1.000	-0.709	-0.802	-0.880	0.552	-0.832	-0.761
A.I.												1.000	0.402	0.533	-0.494	0.482	0.586
ROS													1.000	0.885	-0.366	0.937	0.491
N/CI														1.000	-0.493	0.823	0.695
ATP/ADP															1.000	-0.543	-0.658
PDH-P/total																1.000	0.600
P-AMPK																	1.000

positive correlation — R^2 0.30, 0.40, 0.50, 0.60, 0.70, 0.80, 0.90, 1.00 — negative correlation

Graphical abstract

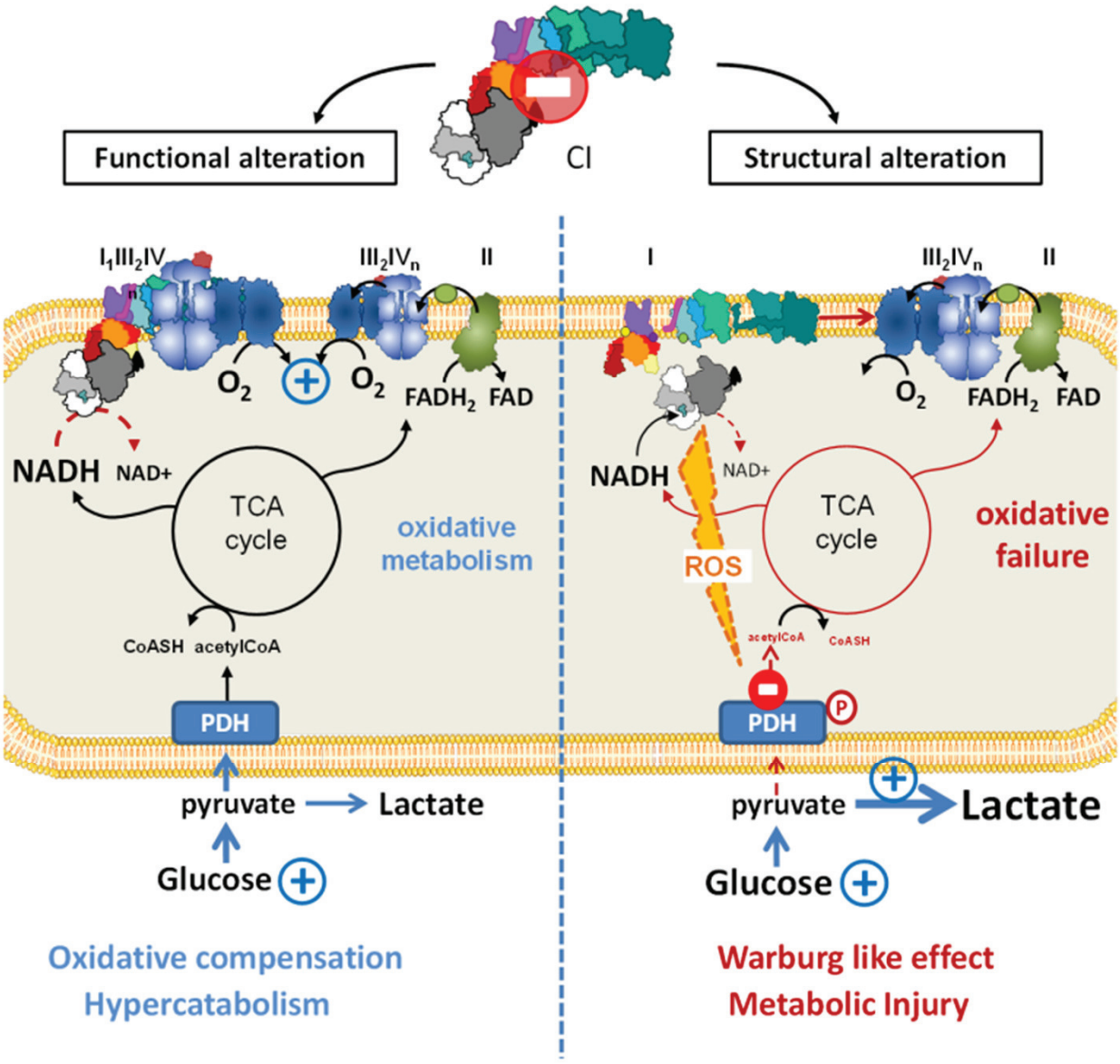

Metabolic reprogramming in CI deficient cells